



# Effectiveness of embedded discontinuities technique in capturing geomechanical behavior in naturally fractured reservoirs

Bruno Maciel<sup>1</sup> · Leidy Laura Alvarez<sup>1</sup> · Nayara Torres Belfort<sup>1</sup> · Leonardo José do Nascimento Guimarães<sup>1</sup> · Leila Brunet de Sá Beserra<sup>1</sup>

Received: 25 June 2023 / Accepted: 22 November 2023 / Published online: 22 December 2023  
© The Author(s) 2023

## Abstract

This paper highlights the efficacy of the finite element method with embedded strong discontinuities in modeling discontinuities in porous media, specifically in the geomechanical behavior of Naturally Fractured Reservoirs (NFRs). The approach considers hydromechanical coupling and offers low computational cost. NFRs account for a significant portion of global reserves, representing approximately 60% of global oil reserves and 40% of gas reserves. Given that flow in NFRs is more complex than in conventional reservoirs due to the presence of multiple fractures, it's crucial to understand how pressure variations or effective stress during operations impact fracture closure and permeability of these reservoirs. To analyze this behavior, numerical simulation results using the proposed method were compared, under different liquid pressure depletion values, with the approach proposed by Oda, which is commonly used in commercial software for calculating fracture permeability tensors. This approach was enriched with Barton's fracture closure formulation and updates on rock matrix porosity and permeability. Four simulations were conducted: Firstly, a hypothetical scenario consistent with Oda's assumptions, where fractures are interconnected and span the entire grid cell, to validate the numerical hydromechanical model; subsequently, three representative sections of a Brazilian pre-salt carbonate reservoir were selected. The study confirms the efficacy of the technique of embedded strong discontinuities in calculating equivalent permeabilities in NFRs, considering geomechanical effects, especially in cells with high fracture frequencies and intensities. Furthermore, the relevance of analyzing the geomechanical behavior in NFRs is emphasized.

**Keywords** Naturally fractured reservoirs (NFRs) · Discrete fracture networks (DFNs) · Embedded strong discontinuities · Equivalent permeability

## List of symbols

$A$	Exponent to be determined experimentally (dimensionless)	$h$	Strain localization band width (m)
$A_{cs}$	Cross-sectional area (m <sup>2</sup> )	$j_n$	Actual closure (m)
$A_k$	Fracture areas (m <sup>2</sup> )	$k$	Permeability (mD)
$E(\mathbf{n})$	Probability density function (dimensionless)	$k_{ij}$	Permeability tensor (mD)
$e^{\varepsilon_{vol}}$	Sum of the normal components of the strain tensor (dimensionless)	$k_o$	Initial matrix permeability (mD)
$F_{ij}$	Fracture tensor (dimensionless)	$ks$	Permeability in the discontinuity (mD)
$F_{kk}$	Principal directions of permeability (dimensionless)	$\mathbf{K}_\Omega$	Permeability tensor of the continuous part (mD)
$f_k$	Percolation factor for fracture (dimensionless)	$\mathbf{K}_{ef}$	Effective permeability tensor for the element (mD)
		$K_{ni}$	Initial normal stiffness (N/m <sup>2</sup> )
		$l$	Length of the section (m)
		$l_e$	Length of the element (m)
		$M$	Matrix obtained from the components of vector $\mathbf{m}$ (dimensionless)
		$\mathbf{m}$	Unit vector normal to the base of the element in the direction of the isolated node (dimensionless)
		$\mathbf{n}$	Unit vector normal to $S_e$ in the direction of $\Omega_e^+$ (dimensionless)

✉ Bruno Maciel  
bruno.canabarro@ufpe.br

<sup>1</sup> Departamento de Engenharia Civil, Universidade Federal de Pernambuco (UFPE), Av. da Arquitetura, s/n, Recife, Pernambuco CEP 50740-550, Brazil

$n_*$	Components of a unit normal vector to fracture (dimensionless)
$N$	Number of fractures (dimensionless)
$N_n$	Matrix obtained from the components of vector $n$ (dimensionless)
$p$	Pressure (Pa)
$q$	Flow rate (m <sup>3</sup> /s)
$q_{ef}$	Effective fluid flow for the element (m <sup>3</sup> /s)
$q_\Omega$	Fluid flow in the continuous part of the element (m <sup>3</sup> /s)
$q_s$	Fluid flow in the discontinuity (m <sup>3</sup> /s)
$S_e$	Strain localization band (dimensionless)
$t$	Discontinuity direction (dimensionless)
$T_k$	Transmissivities (m <sup>2</sup> /s)
$\llbracket \mathbf{u} \rrbracket$	Jump in the displacement field (m)
$V$	Volume of the grid cell (m <sup>3</sup> )
$V_m$	Maximal closure of the fracture aperture (m)
$\delta_{ij}$	Kronecker delta (dimensionless)
$\Delta P$	Pressure difference (Pa)
$\varepsilon$	Regular strain field (dimensionless)
$\varepsilon_S$	Strain field at the strain localization band (dimensionless)
$\varepsilon_\Omega$	Strain field in the continuous portion (dimensionless)
$\varepsilon_S^0$	Initial strain field (dimensionless)
$\mu$	Viscosity (m <sup>2</sup> /s)
$\rho$	Density (kg/m <sup>3</sup> )
$\sigma_\Omega$	Stress field in the continuous part of the element (Pa)
$\sigma_S$	Stress field in the strain localization band (Pa)
$\sigma_n$	Component of the stress tensor normal to fracture (Pa)
$\Sigma$	Constitutive matrix of the material (dimensionless)
$\phi$	Porosity (dimensionless)
$\phi_0$	Porosity of the rock matrix in the reference configuration (dimensionless)
$\Omega_e$	Domain of the element (dimensionless)

## Introduction

Fractured geological formations are found worldwide and pique the interest of various researchers in fields such as aquifer exploration and contamination, oil reservoir exploration, geothermal reservoir exploration, heat storage, among others (Bear et al. 1993; Sahimi 1995; National Research Council 1996, 2001; Evans et al. 2001; Berkowitz 2002).

Within the context of oil reservoir exploration, naturally fractured reservoirs (NFRs) hold a distinct position. According to Spence et al. (2014), NFRs are underground geological formations that contain hydrocarbons (oil and natural gas) and are characterized by the presence of natural

fractures or fissures. These fractures can result from various geological processes, such as the movement of tectonic plates, structures formed by thermal contraction during the cooling of volcanic rocks, or the accumulation of stress in layers of sedimentary rock that eventually lead to ruptures or fractures.

The importance of NFRs becomes evident when considering that they represent approximately 60% of global oil reserves and 40% of global gas reserves (Ahmed 2014). Therefore, it becomes essential to conduct a precise characterization of the fracture network properties to optimize the modeling and simulation of these reservoirs (Haridy et al. 2019). Furthermore, the efficiency of recovery in NFRs is directly influenced by the increased permeability due to the presence of natural fractures in these systems (Golf-Racht 1982; Ghahfarokhi and Wilson 2015).

Advancements in understanding flow in Unconventional Reservoirs have been remarkable. Many studies highlight that flow in these reservoirs is more complex when compared to conventional reservoirs. Sarma and Aziz (2006) emphasize that this complexity arises from the presence of multiple fractures or fault systems within the rock, supported by Pan et al. (2010).

The characterization of these flow structures, in turn, is not straightforward. While some can be defined using geophysical and hydraulic methods, many others require statistical approaches. In certain applications, such as in estimating effective permeability, detailed knowledge of the flow structure may not be essential. This is indicated by studies by Yeh and Liu (2000), Rubin and Hubbard (2005), and Dreuzy et al. (2012).

However, when addressing the modeling of NFRs, there arises a need to discern which fracture properties are crucial for fluid flow and transport. In this context, the approach of Discrete Fracture Networks (DFN) takes center stage. DFN is designed to emulate the fractured environment on a reduced scale, ensuring, however, that the individual characteristics of each fracture are faithfully represented.

Initially, DFN were developed to model smoothed fractured media (Long et al. 1982), and they were subsequently applied to understand flow structures in complex fracture networks (Dreuzy et al. 2001; Leung and Zimmerman 2010; Le Goc et al. 2010; Pichot et al. 2010), increase permeability and dispersivity (Charlaix et al. 1987; Dreuzy et al. 2001, 2010; Baghbanan and Jing 2007; Frampton and Cvetkovic 2007, 2009), and define the correct modeling approach (Long et al. 1985; Sahimi 1993; Davy et al. 2006; Jourde et al. 2007; Cello et al. 2009; Ji et al. 2011). DFN can extract important information about flow properties from extensive geological and geophysical data available in the fractured medium (Bonnet et al. 2001; Davy et al. 2010).

The initial three-dimensional (3D) stochastic simulations of DFN were developed as a proof of concept (Long et al. 1985; Dershowitz and Fidelibus 1999). These simulations demonstrated the wide range of transport transit times within a given fracture network, as well as the differences in average times obtained from different simulations (Nordqvist et al. 1996). They also indicated the possibility of excluding smaller fractures from networks dominated by larger fractures (Wellman et al. 2009). However, 3D stochastic modeling of DFN faced challenges, primarily in generating high-quality meshes using classical mesh algorithms (Maryška et al. 2004; Kalbacher et al. 2006).

3D flow simulations in complex fracture networks required changes in geometric configurations, which could compromise mesh quality throughout the structure (Erhel et al. 2011). These challenges have limited the efficient application of 3D stochastic DFN modeling. However, ongoing research is addressing these limitations by exploring advanced mesh generation approaches, such as the embedded strong discontinuities technique and pseudo-coupling methods. These advances are essential for improving the accuracy and efficiency of flow simulations in complex fracture networks.

The analysis of Discrete Fracture Networks (DFN) is important in the development of hydromechanical models that consider the discrete characteristics influencing fluid flow. Understanding the nature of transport paths within these features and their barriers to flow is essential, as it directly impacts the modeling accuracy. Without this understanding, reliable results cannot be achieved. In this context, the analysis of DFN holds fundamental significance, helping create models that capture the complexity of fracture networks and adequately represent fluid flow behavior. By considering both known and unknown fracture characteristics, it is possible to enhance the precision and reliability of results in various applications, such as natural resource exploration and environmental risk assessment.

The choice of the appropriate technique for analyzing permeability in a DFN model is important for the recovery of naturally fractured reservoirs. According to Haridy et al. (2019), two commonly used methods are numerical flow-based simulation and the analytical approach, known as the Oda method.

The first method, flow-based numerical simulation, is highly accurate as it considers details of flow within individual fracture channels. However, this approach is computationally demanding because it requires simulating each fracture individually. Therefore, its use may be limited in terms of processing time and available computational resources.

On the other hand, the analytical approach, or the Oda method, is computationally efficient. In this method, permeability is calculated based on information about

fracture geometry, such as aperture, size, and orientation. However, it is important to note that the Oda method is more suitable for well-connected fracture networks that span the entire grid cell. In cases of less connected or partially connected fracture networks, the Oda method may not provide accurate results.

Therefore, when choosing between flow-based numerical simulation and the analytical approach, it is necessary to consider the desired accuracy, available computational resources, and the connectivity of the fracture network under study. Careful selection of the appropriate technique will enable a more reliable estimation of permeability, contributing to the optimization of recovery in naturally fractured reservoirs.

A widely accepted and applied approach for efficiently simulating the propagation of fractures in concrete structures is the finite element method with embedded strong discontinuities. This technique can be properly adapted to simulate the propagation and closure of fractures in saturated porous media, considering hydromechanical coupling (Beserra et al. 2016).

One of the advantages of this technique is the elimination of the need for interface elements or geometry trimming, as required in conventional discrete fracture methods. This significantly simplifies the modeling process, reducing the complexity and computational time required to obtain reliable results. Furthermore, embedded strong discontinuities are in accordance with the principles of continuum mechanics, ensuring greater consistency with the physical properties of porous media. This enhances the accuracy of simulation results, making them more representative of the material's physical behavior. Another advantage of this technique is the reduction in computational costs associated with discretizing the fractured medium. By avoiding the necessity for additional interface elements, the number of finite elements needed to represent the fractured medium is significantly reduced. This results in a computationally more efficient model, expediting the simulation process and allowing for the analysis of larger-scale systems.

Thus, the use of embedded strong discontinuities in the context of numerical simulation with the finite element method provides an efficient and accurate alternative for modeling discontinuities in porous media, such as fractures in geological formations. This approach combines the simplicity of the continuous approach with the ability to precisely represent the behavior of discontinuities, making it a valuable choice for various engineering applications.

On the other hand, Oda (1985) developed a theory that treats discontinuous rock masses as homogeneous and anisotropic porous media. In this theory, the permeability tensor is formulated based on measurable quantities obtained in situ, such as fracture orientation data (Oda et al. 1989).

The proposed approach calculates the permeability tensor by considering the fracture tensor, which is determined by the fracture geometry, including aperture, size, and orientation. This approach is widely used in commercial software to compute fracture permeability tensors and is recognized as a fast algorithmic method (Ghahfarokhi 2017). It is important to note that this approach assumes that all fractures are connected, which can lead to an overestimation of effective permeability. Therefore, in situations where fractures are not fully connected, the Oda method may result in an inaccurate estimate of effective permeability (Dershowitz et al. 2000; Gupta et al. 2001; Decroux and Gosselin 2013).

The overestimation of permeability is a significant concern in various geological and reservoir engineering contexts as it can lead to inaccurate and sometimes overly optimistic predictions. Some of the issues associated with the overestimation of permeability include:

*Inaccurate predictions and poor well development:* In oil and gas reservoirs, the accurate estimation of permeability is crucial for proper well development, including determining drilling locations and selecting recovery methods. Overestimation can lead to inadequate development decisions. As noted by Fowler (2019), when permeability is overestimated, production projections tend to be overly optimistic. This, in turn, can result in inefficient resource allocation and improper sizing of wells and clusters in oil and gas production projects.

*Overestimated storage capacity:* In scenarios involving underground fluid storage, such as CO<sub>2</sub> or natural gas, overestimating permeability can lead to a misguided assessment of the actual fluid storage capacity underground. This inaccuracy has significant implications for the planning and safety of these projects. According to Thibeau and Mucha (2011), during large-scale geological storage of CO<sub>2</sub> in the future, it is imperative that the pressure increase remains below specified values to ensure safe and long-term containment of CO<sub>2</sub> at the storage site.

*Pressure issues:* The overestimation of permeability can result in an underestimation of reservoir pressure, which, in turn, can lead to unsafe or inefficient operations and the unwanted release of fluids to the surface. According to Gao and Flemings (2017), if reservoir pressure is underestimated, there may be a rapid inflow into the well (i.e., a 'kick'), while an overestimation of reservoir pressure can lead to well overdesign and fluid outflow (i.e., 'lost circulation') in some cases.

Therefore, accurate permeability estimation is essential for effective planning and operations in many fields of geology, reservoir engineering, and natural resource management. The overestimation of permeability can result in significant issues and additional costs.

More recent approaches have been developed to address variability in fracture connectivity and overcome the

limitations of the Oda method. These approaches consider the presence of unconnected fractures and consider the influence of the fracture network on effective permeability more accurately. An example is the work of Dershowitz et al. (2000), who developed an empirical estimation of the fracture tensor using a weighted combination of fracture area and transmissivity. This approach allowed for obtaining permeability values closer to those obtained by the traditional method, and in some situations, permeabilities below the percolation threshold were found when the fracture length was significant.

It is also important to note that the topology of fractures can have different impacts on fluid flow in naturally fractured media. Studies such as Jing and Stephansson (1997) and Sævik and Nixon (2017) have investigated the influence of the fracture system's geometry on fluid flow analysis. Alvarez et al. (2021) analyzed the impact of hydraulic connectivity, related to fracture topology, on the behavior of flow properties, including permeability. Despite these advances, simulations in scenarios closer to reality showed that analytically corrected methods using topological analysis were not efficient in estimating the equivalent permeability of fractured media. This highlights the complexity and challenges involved in accurate and reliable modeling of permeability in discontinuous porous media.

As mentioned earlier, a significant portion of hydrocarbons is found in naturally fractured reservoirs (NFR), often considered as equivalent continuous porous media, neglecting the impact of fractures on fluid flow and geomechanics (Zareidarmiyan et al. 2018). However, this simplification appears inadequate in certain situations, especially in carbonate reservoirs, where a substantial portion of conventional oil and gas reserves is in highly fractured carbonate rocks (Nelson 2001; Narr et al. 2006).

To support this assertion, studies conducted by Li et al. (2015) and Yan et al. (2018) demonstrated that the presence of natural fracture networks results in complex flow patterns and concentration of stresses and deformations in reservoirs. This behavior occurs because fractures control the mechanical response of fractured rock, act as preferential pathways for fluid transport, and are more sensitive to changes in stress (Gutierrez and Youn 2015; Shin and Santamarina 2019; Mejia et al. 2022).

According to Couples (2014), the role of geomechanics in fractured reservoirs is more complex than suggested, as illustrated by numerical simulations demonstrating the occurrence of intense nonlinear interactions between fluids and geomechanics. The resulting movements within fractured rock masses can cause significant changes in flow properties. While an individual fractured reservoir may exhibit a real flow response during production that closely matches predictions, there is often a wide variation in flow behavior. Couples (2014) goes as far as to state that

experienced engineers and geologists seem to operate with the expectation that fractured reservoirs will have some surprises. Some of these "surprises" occur frequently enough to become expectations, such as steep decline curves, water breakthrough anticipation, and unusual interference patterns.

From a geomechanical perspective, it is expected that interactive fractured systems exhibit variations in fracture apertures along each fracture face, especially during transient events such as reservoir operations. However, as noted by Dreuzy et al. (2012), limited efforts have been made to simultaneously model the effects on fracture apertures and the complex network structure. Dreuzy et al. (2012) refer to studies in which the initial approach involves treating fractures, which exhibit heterogeneity, as parallel plates with the same equivalent transmissivity. However, this approach appears inadequate, as fluid flow can exploit variations in fracture apertures as well as high transmissivity shortcuts in the network.

Fracture apertures vary in time and space, depending on the expected system behavior. These variations can trigger significant changes in the fracture network's topology, which, in turn, has substantial implications for fluid flow. In extreme situations, as highlighted by Dreuzy et al. (2012), the closure of a fracture can disconnect hydraulic pathways, resulting in a reorganization of flow within the network. Therefore, it is essential to employ a three-dimensional model that considers both the heterogeneity in fracture geometry and the complex arrangements within the network.

Considering the interaction between fluids and geomechanics in naturally fractured reservoirs can have a significant impact on flow properties and reservoir behavior. Faults and fractures are present in virtually all deep-seated rocks, and their influence extends to fluid transport, mechanical properties, and wellbore stability (Zoback 2007).

Lei et al. (2017) emphasize the importance of not only geometrically representing discontinuities in three-dimensional fractured rock systems but also considering the complex hydromechanical interactions. These hydromechanical processes become notably more complex when natural fractures are involved (Zimmerman and Main 2004; Latham et al. 2013). The existence of fractures has the potential to affect rock mass permeability and, thus, influence fluid migration (Rutqvist and Stephansson 2003).

According to Longuemare et al. (2002), geomechanical effects can be especially pronounced in certain types of reservoirs, such as those with low compactness or fractures. In low-compactness reservoirs, variations in stress can enhance fluid recovery due to reservoir compaction. However, this compaction can also result in reduced permeability, leading to surface subsidence and wellbore equipment damage. These effects can only be adequately explained through a highly sophisticated geomechanical analysis, which necessarily incorporates elements such as

constitutive behavior that captures the effects of fracture opening and closing, water weakening effects, stress trajectory, and considerations of initial stress conditions.

This careful consideration of changes in rock porosity and fracture apertures is especially important in fractured reservoirs, where complex interactions between fluids and geomechanics can significantly impact flow properties. The embedded strong discontinuities technique allows for a better characterization of fractured reservoirs and can be valuable in making decisions related to hydrocarbon exploration.

The objective of this article is to demonstrate the efficacy of using embedded strong discontinuities technique as an efficient and accurate alternative for modeling discontinuities in porous media, such as in naturally fractured reservoirs, considering the hydromechanical coupling.

To achieve the proposed objective, a Python routine was developed to calculate the equivalent permeability of the fracture network, using the Oda approach dynamically for three-dimensional DFN cells. For this, Oda's methodology was combined with the fracture closure formulation of Barton & Bandis, and incorporated updates to the porosity and permeability of the porous medium. Thus, it was obtained analytical results that could be compared with the results of numerical simulations using the embedded strong discontinuities method. Four simulations were performed: First, a hypothetical scenario consistent with Oda's assumptions, where the fractures are interconnected and span the entire grid cell, was established to validate the numerical hydromechanical model. Subsequently, three representative sections of an offshore carbonate reservoir in the pre-salt layer, investigated by Petrobras in Brazil, were selected. Each section exhibits varying intensities of fracture. In carbonate scenarios A, B and C, Oda's assumptions that the fractures are interconnected and cover the entire cell are not valid.

Three-dimensional simulations were conducted using the finite element software CODE\_BRIGHT, in which the embedded strong discontinuities technique is implemented (Olivella et al. 1994, 1995; Guimarães et al. 2007). This technique stands out from other methods due to its numerous advantages. It eliminates the need for interface elements, leading to a reduction in the number of required finite elements and subsequently simplifying the modeling process. This efficiency reduces computational complexity and time, optimizing the simulation for analyzes of large-scale systems or those with a high number of fractures. Although it has a longer computational time compared to analytical approaches, this technique aligns with the principles of continuum mechanics, ensuring more accurate and true-to-life results.

In this way, the use of embedded strong discontinuities in the context of numerical simulation with the finite element method offers an efficient and accurate alternative for



modeling discontinuities in porous media, such as fractures in geological formations. This approach combines the simplicity of the continuum approach with the ability to accurately represent the behavior of discontinuities, making it a valuable choice for various applications in engineering and earth sciences.

## Theoretical background

### Discrete fracture models

Discrete fracture models provide the ability to quantify many flow and transport phenomena that are not adequately captured by continuous models. One of the main advantages of the discrete fracture approach is its ability to explicitly incorporate the effects of individual fractures on fluid flow and solute transport, which allows a more accurate representation of the actual fractures' behavior.

These models have become increasingly popular in theoretical studies and practical applications due to their advantages over continuous models. However, it is important to note that the practical application of these models may be limited if detailed field data is not available. Calibration and validation of these models require a greater amount of data compared to continuous models due to the complexity of fractures and their influence on flow and transport behavior. Each individual fracture has unique characteristics such as orientation, conductivity, and connectivity, which locally affect fluid flow and solute distribution. Therefore, to obtain accurate and reliable results, it is crucial to have detailed information about the fractures present in the studied system.

Discrete fracture models are a powerful tool for studying flow and transport in fractured systems, allowing for a more realistic and accurate representation of these phenomena. However, it is important to consider computational limitations and the need for detailed field data when applying these models in practical contexts. Most approaches currently used for simulating flow in reservoirs with natural fractures can be divided into two main strategies: continuous models and discrete fracture models, also known as Discrete Fracture Networks (DFN) (Berkowitz and Balberg 1993).

In DFN approach, fluid flow is directly simulated within the fractures, allowing the incorporation of various characteristics of real fracture systems already mentioned, whose is capable of handling complex fracture geometries. It allows detailed and accurate representation of fractures, while, in continuous models approach, flow within the fractures is not directly simulated but is represented through blocks in a grid. For each block, an equivalent

permeability is calculated, considering the average effect of the fractures present. One advantage of continuous models is their ability to simulate more complex recovery mechanisms, such as capillary pressure and interactions between the rock matrix and fractures (Niven and Deutsch 2009).

It is important to highlight that both approaches have their specific limitations and advantages. The DFN approach is more suitable for theoretical studies and detailed analyzes, while continuous models are more applicable in larger-scale situations. Choosing between these approaches depends on the specific needs of the study and the accessibility to data and computational resources.

About hydraulic head gradient, fluid flow in fractured rocks varies heterogeneously throughout the domain, primarily within the fractures, where flow is influenced by the orientation, conductivity, and connectivity of the fractures, then in the rock matrix, where flow is determined by the permeability of the matrix and the ability of the fracture network to allow pressure gradients within matrix blocks.

The combined behavior of fractures and the matrix results in a specific volumetric flow, representing the interaction between these two parts of the rock. Block permeability, or equivalent permeability, is the proportionality factor relating the pressure gradient of the block to the total flow. This permeability is a measure of flow efficiency within a fractured rock block.

It is important to highlight the distinction between block permeability and effective permeability, since the block permeability considers the individual characteristics of fractures and the matrix, while effective permeability is an average measure that considers a representative elementary volume of the rock. However, in fractured rocks, it is challenging to define this elementary volume due to the fractal nature of fracture geometry and a common lack of an appropriate homogenization scale. The permeability of fractured rock is not an intrinsic and uniform property, but one that varies significantly with scale and the considered sample, however, it is needed to be considered when studying fluid flow in fractured rocks (Lang et al. 2014).

Fractured rocks can exhibit anisotropic permeability determined by the aperture, length, and orientation of the open fractures. Due to the strong influence of fracture aperture on fluid flow, the stress effect on the permeability of fractured rocks can be of great importance.

It implies that stress characteristics in rocks, such as the direction and magnitude of stresses, can affect fracture permeability and, in turn, fluid flow. When subjected to different stress states, fractures can open or close, altering the connectivity and efficiency of fluid flow through the

fractured rock. Thus, understanding the behavior of fractures in response to stress is fundamental for properly assessing permeability and flow in these rocks.

The importance of stress on the permeability of fractured rocks emphasizes the need to consider geomechanical effects when modeling and predicting fluid flow behavior, which is essential in various fields, such as petroleum reservoir engineering, geothermal resource exploration, and groundwater management (Sayers 1990).

### Finite element with embedded discontinuities

To represent the behavior of fractures in a rock formation, it was adopted the embedded strong discontinuity approach, which allows incorporating the effect of a deformation band within the existing finite elements. This approach, as described by Beserra et al. (2018), has been implemented in CODE\_BRIGHT, a finite element software that performs fully coupled numerical analysis of fluid flow in a deformable porous medium.

Embedded strong discontinuity is a powerful technique that captures the behavior of fractures in the finite element model, enabling a more accurate representation of deformations and interactions between the fluid and fractures. By introducing the effect of the discontinuity within the finite elements, the model becomes capable of simulating interactions between the deformable rock matrix and fractures, considering the influence of fracture deformation and aperture on fluid flow. This provides a more realistic and precise representation of the system's behavior.

To properly derive the formulations of finite elements with embedded discontinuities, it is important to consider fundamental aspects related to the kinematics and statics of the discontinuity. The kinematics should accurately represent the position of the interface within the element, as well as the relative displacement (aperture and sliding) between the opposing faces of the interface. Additionally, the continuity of traction condition should be correctly applied to establish an accurate relationship between the tractions at the internal interface and the stresses in the surrounding continuous portion. These considerations are essential to ensure the accuracy and consistency of the results obtained when using embedded discontinuities in finite element analyzes.

The incorporation of this technique into finite element code is highly convenient and can be performed in a non-intrusive manner within the code. The jump in the displacement field can be approximated as equivalent inelastic deformations, which can be calculated within the constitutive module of the finite element program during the stress integration process in the elements.

The equations of finite elements without discontinuities are used to represent the continuous part of the problem. However, to model the behavior of the discontinuity

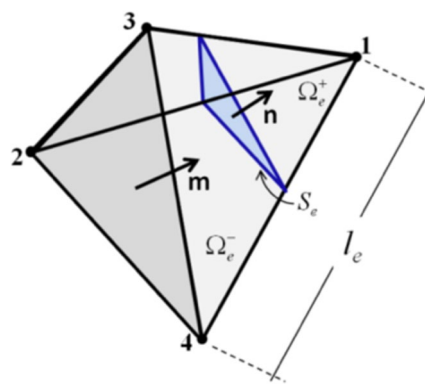


Fig. 1 Finite element crossed by a discontinuity band

interface, an additional approach is required. One option is to employ a constitutive equation that directly relates the stresses and displacements at the discontinuity interface. Alternatively, a continuous constitutive model can be used, which relates the stresses and strains considering the continuous approximation of the strong discontinuities (Manzoli and Shing 2006).

Consider a tetrahedral element with four nodes belonging to the domain  $\Omega_e$ . The length of this element is represented by  $l_e$ . This element has a strain localization band, denoted as  $S_e$ , which divides the element into two distinct parts. The strain band has a width  $h$  and isolates node 1 from nodes 2, 3, and 4, as illustrated in Fig. 1.

The jump in the displacement field,  $[[\mathbf{u}]]$ , in the region  $S$  results in a rigid relative movement. The strain field in the continuous portion and in the discontinuity can be expressed as:

$$\epsilon_{\Omega} = \epsilon - \frac{1}{l_e} M [[\mathbf{u}]] \tag{1}$$

$$\epsilon_S = \epsilon - \frac{1}{l_e} M [[\mathbf{u}]] + \frac{1}{h} N_n [[\mathbf{u}]] \tag{2}$$

The corresponding stress field is given by:

$$\sigma_{\Omega} = \Sigma(\epsilon_{\Omega}) = \Sigma(\epsilon - \frac{1}{l_e} M [[\mathbf{u}]] \tag{3}$$

$$\sigma_S = \Sigma(\epsilon_S) = \Sigma(\epsilon - \frac{1}{l_e} M [[\mathbf{u}]] + \frac{1}{l_e} N_n [[\mathbf{u}]] \tag{4}$$

where  $h$  denotes the bandwidth of strain localization,  $\Sigma$  is the constitutive matrix of the material;  $M$  and  $N_n$  are the matrices obtained from the components of vectors  $\mathbf{m}$  and  $\mathbf{n}$  respectively and  $[[\mathbf{u}]]$  is the jump in displacement field. Traction continuity is assured as follows:

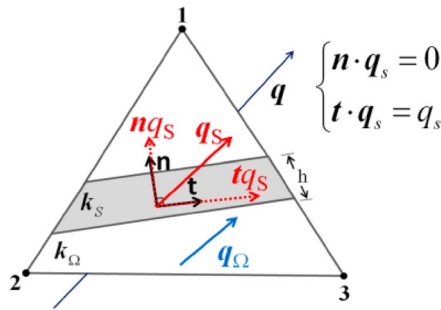


**Fig. 2** The normal and Tangential component of fluid flow in discontinuity

$$N_n \cdot (\sigma_\Omega - \sigma_s) = 0 \tag{5}$$

**Flow problem**

Darcy flow in the discontinuity can be decomposed into a normal and tangential component, as illustrated in Fig. 2.

The formulation used in this paper considers that the fluid flow in a fracture occurs on its direction, therefore only the tangential component is considered. Darcy’s law can be written, for continuum and fracture, as follows:

$$q_\Omega = -K_\Omega \nabla p \tag{6}$$

$$q_s = -\frac{h}{l_e} k_s t \otimes t \nabla p \tag{7}$$

As the fracture becomes a preferential pathway for flow toward the discontinuity in a porous medium, this can be interpreted as induced anisotropy in the direction of the fracture throughout the medium. As a result, the effective permeability of the element is given by:

$$q_{ef} = -K_{ef} \nabla p \tag{8}$$

$$K_{ef} = \left( K_\Omega + \frac{h}{l_e} k_s t \otimes t \right) \tag{9}$$

**Update of the porosity and permeability of the fractured porous medium**

A simulation of reservoir behavior is based on the conservation of mass of the species contained within it. In the case of considering geomechanical coupling, the reservoir rock becomes deformable, and the variation in its porosity is calculated from the conservation equation of solid phase mass and the volumetric deformation of

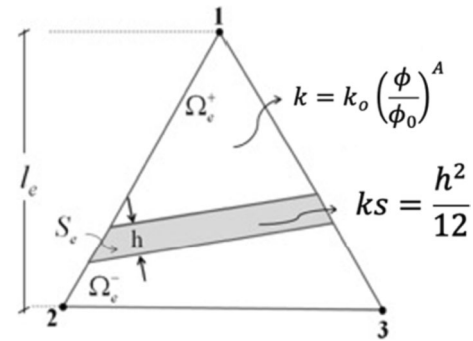


**Fig. 3** Permeability Variation laws for parent rock and discontinuity

the medium. Porosity can be determined as a function of volumetric deformation in the following way:

$$\phi = 1 - (1 - \phi_0) e^{\epsilon^{vol}} \tag{10}$$

In this equation,  $\phi_0$  represents the porosity of the rock matrix in the reference configuration, and  $e^{\epsilon^{vol}}$  is the sum of the normal components of the strain tensor.

In addition to the variation in porosity, there will also be a change in rock permeability. For the intact rock, it is adopted a law of permeability variation proposed by Falcao et al. (2018):

$$k = k_o \left( \frac{\phi}{\phi_0} \right)^A \tag{11}$$

where  $k_o$  denotes the initial matrix permeability,  $\phi$  the porosity calculated after perturbations induced by rock deformation and  $A$  a proper exponent to be determined experimentally.

Two different permeability variation laws, one for parent rock and one for fracture, are adopted as shown in Fig. 3.

It is important to highlight that the CODE BRIGHT finite element program solves the mechanical and fluid flow problems in a fully coupled manner. In each Newton–Raphson iteration, a single system of equations is solved for the entire mesh. The unknowns in the hydraulic solutions are the pressures, while in the mechanical solutions, they are the displacements.

The update of the fracture permeability is determined by the displacement jump from the mechanical problem in the hydromechanical coupling. This update follows the following relationships:

$$k_s = \frac{h^2}{12} \tag{12}$$

where  $h$  is the normal aperture, calculated by:

$$h = V_m - j_n \tag{13}$$



where  $V_m$  is the maximal closure of the fracture, a Barton's model parameter and  $j_n$  is the actual closure.

### Closure constitutive model

To model the mechanical behavior of the material, a hyperbolic fracture closure model proposed by (Barton et al. 1985) was adopted. The normal stress on the fracture is obtained as follows:

$$\sigma_n = \mathbf{n} \cdot \boldsymbol{\sigma}_s \cdot \mathbf{n} \quad (14)$$

The normal closure is obtained from the Barton-Bandis hyperbolic model, which describes the relationship between the normal stress  $\sigma_n$  and the maximum closure of the fracture  $V_m$ . The initial normal stiffness  $K_{ni}$  is also considered in this model.

$$j_n = \frac{\sigma_n V_m}{K_{ni} V_m + \sigma_n} \quad (15)$$

$$j_n = \frac{K_{ni} V_m g_n}{V_m - g_n} \quad (16)$$

The displacement jump vector  $[[\mathbf{u}]]$  is calculated by multiplying the normal closure  $j_n$  by the fracture normal vector  $\mathbf{n}$ .

$$[[\mathbf{u}]] = j_n \mathbf{n} \quad (17)$$

Finally, the deformation field in the discontinuity  $\varepsilon_S$  is determined by combining the term related to the displacement jump  $M[[\mathbf{u}]]$  and the term related to the tangential deformation  $N[[\mathbf{u}]]$ , along with the initial deformation field  $\varepsilon_S^0$ , which corresponds to the deformation induced by the initial stress state of the material.

$$\varepsilon_S = \varepsilon - \frac{1}{l_e} M[[\mathbf{u}]] + \frac{1}{h} N[[\mathbf{u}]] + \varepsilon_S^0 \quad (18)$$

### Oda tensor approach

The Oda approach presents an efficient method for calculating the equivalent permeability of fractures analytically. This method is widely used in solving Discrete Fracture Network (DFN) systems due to its effectiveness. One of the advantages of the Oda approach is that it allows obtaining properties of grid cells directly based on the geometry and properties of the fractures contained within those cells.

The Oda procedure starts by generating a complete three-dimensional DFN. While flow and transport modeling in DFN is limited to approximately  $10^4$  to  $10^5$  fractures due to computational constraints, the Oda approach can be

applied to sets of  $10^7$  fractures or more. The orientation of fractures in each grid cell is expressed by a unit normal vector  $\mathbf{n}$ . By integrating the fractures with respect to all normal vectors, Oda obtains the mass moment of inertia of the fracture normal vectors distributed over a unit sphere:

$$N = \int_{\Omega/2} n_i n_j E(\mathbf{n}) d\Omega \quad (19)$$

where  $N$  is number of fractures in  $\Omega$ ,  $n_i, n_j$  is the components of a unit vector, normal to the fracture plane,  $\mathbf{n}$ ,  $E(\mathbf{n})$  is a probability density function that describes the number of fractures whose unit vectors  $\mathbf{n}$  are oriented within a small solid angle  $d\tilde{\Omega}$  and  $\tilde{\Omega}$  is entire solid angle corresponding to the surface of a unit sphere.

For a specific grid cell with known fracture areas,  $A_k$ , and transmissivities,  $T_k$ , obtained from the DFN model, an empirical fracture tensor relating only to the fracture geometry can be calculated by adding the individual fractures weighted by their areas and transmissivities:

$$F_{ij} = \frac{1}{V} \sum_{k=1}^N f_k A_k T_k n_{ik} n_{jk} \quad (20)$$

In this equation,  $F_{ij}$  represents the fracture tensor,  $V$  is the volume of the grid cell,  $N$  is the total number of fractures in the cell,  $f_k$  is the percolation factor for fracture  $k$  (typically assumed as 1),  $A_k$  is the area of fracture  $k$ ,  $T_k$  is the transmissivity of fracture  $k$ , and  $n_{ik}, n_{jk}$  are the components of a unit normal vector to fracture  $k$ .

The Oda permeability tensor expresses the flow through the fracture as a vector along the unit normal of the fracture. Assuming that the fractures are impermeable in a direction perpendicular to the fracture plane, it is necessary to rotate the  $F_{ij}$  tensor to the permeability planes. This rotation is performed using the Kronecker delta,  $\delta_{ij}$ , to normalize the orientation of fractures with respect to the control volume (Dershowitz et al. 2004; Elfeel 2014). The formula for calculating the permeability tensor  $k_{ij}$  is given by:

$$k_{ij} = \frac{1}{12} (F_{kk} \delta_{ij} - F_{ij}) \quad (21)$$

where  $F_{ij}$  is the fracture tensor, and  $F_{kk}$  are the principal directions of permeability. It is worth noting that the Oda tensor approach is a way to balance accuracy when modeling each of the structures in the model with computational efficiency by using coarser discretizations. However, for distances of tens or hundreds of meters, the results obtained from the Oda approximation may be less accurate (Dershowitz et al. 2004).

As mentioned earlier, the Oda permeability tensor calculates permeability by considering only fluid flow in a rigid porous medium. The idea of this research is to

develop a method for obtaining the Oda permeability tensor by incorporating geomechanics in fractures and the parent rock, to compare the results with those obtained through numerical simulation.

## Methodology

This study highlights the effectiveness of the finite element method with embedded strong discontinuities in modeling discontinuities in porous media, focusing on hydromechanical coupling in NFR (Natural Fractured Reservoir) simulations.

The experiment involves hydromechanical simulations in three-dimensional DFN (Discrete Fracture Network) cells using the CODE\_BRIGHT finite element software, where the embedded strong discontinuities technique was implemented as detailed in Sect. “Finite element with embedded discontinuities”. One of the advantages of this technique is the elimination of the need for interface elements or geometric cutout, common requirements in traditional discrete fracture simulation methods. In this method, fractures are directly incorporated into the existing mesh elements. This significantly simplifies the fracture network modeling process, resulting in a reduction in complexity and computational time required to obtain reliable results. By avoiding the use of additional interface elements, a more efficient computational model is created, speeding up the simulation process and enabling the analysis of larger-scale systems.

To model the mechanical behavior of fractures was adopted the hyperbolic fracture closure model proposed by Barton et al. (1985), as described in Sect. “Closure constitutive model”. To represent the rock matrix, standard finite elements and linear elastic constitutive model were used. To ensure hydromechanical coupling, the normal closure of the fracture is determined by the jump in the

displacement field obtained from the strong discontinuity approach.

The adopted methodology involves subjecting the samples to constant vertical tension throughout the simulation, with lateral displacement restrictions, as illustrated in Fig. 4a. These restrictions ensure that the sample remains entirely fixed, without deformations at the sides or the base. Equivalent properties, such as permeability, are calculated for various flow directions. These calculations are performed by applying a pressure gradient of  $\Delta P = 0.1$  MPa between points P1 and P2, as illustrated in Figs. 4b for horizontal orientations and 4(c) for vertical orientations.

Equivalent properties are determined at various levels of pore pressure depletion, ranging from 55 to 10 MPa, with reductions of 5 MPa at each stage. The duration of the pressure gradient application is based on the time required for the samples to reach a steady state, a fundamental requirement for the accurate evaluation of equivalent permeability. Steady state is reached when the flow at the sample inlet and outlet stabilizes, becoming constant over time. This means that there are no longer significant variations in the flow rate or other properties of the system, indicating that the internal conditions of the sample have reached a dynamic equilibrium. At this point, the total flow rate along the boundary is calculated to determine the equivalent permeability of the medium. This calculation considers the permeabilities and properties of fractures and the rock, as expressed in the following equation:

$$k = \frac{\mu l q}{\rho A_{cs} \Delta P} \quad (22)$$

where  $k$  represents the equivalent permeability,  $\mu$  is viscosity,  $l$  denotes the length of the section,  $q$  refers to the flow rate,  $\rho$  represents density,  $A_{cs}$  is the cross-sectional area, and  $\Delta P$  indicates the pressure difference.

To contrast the results of the numerical simulations, considering various liquid pressure depletion values, with the approach proposed by Oda, commonly employed in commercial software to compute fracture permeability tensors, a Python routine was developed. This routine dynamically calculates the equivalent permeability of the fracture network using Oda tensor approach (sect. “Oda tensor approach”), enhanced with closure constitutive model by Barton & Bandis (Sect. “Closure constitutive model”), and updates on rock matrix porosity and permeability (Sect. “Update of the porosity and permeability of the fractured porous medium”). These adjustments in fracture openings and matrix properties are pre-computed in the routine for each pressure level. The updated opening values are incorporated into Oda's approach to determine the fracture network's equivalent permeability, which is then added to the permeability updates computed for the

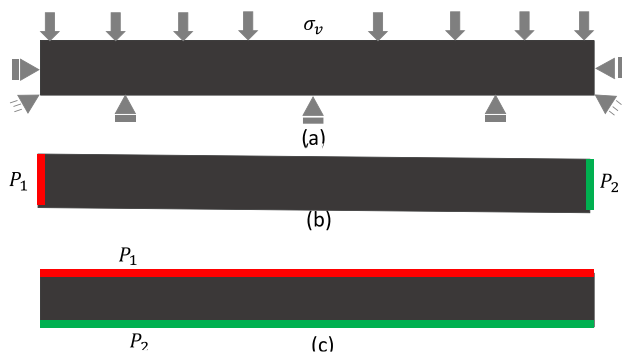


**Fig. 4** Boundary conditions: **a** Effective stress and mechanical conditions **b** Hydraulic boundary condition to obtain horizontal permeability **c** Hydraulic boundary condition to obtain vertical permeability

**Table 1** Rock and fracture properties

Vertical permeability (mD)	0.026
Horizontal permeability x and y (mD)	343.2
Height (m)	10
Width (m)	200
Long (m)	200
Specific Mass (kg/m <sup>3</sup> )	2360
Poisson's ratio	0.3
Young's modulus (GPa)	16.9
Fracture normal stiffness (MPa/m)	12,041
Fracture tangential stiffness (MPa/m)	5557
Initial pressure (MPa)	55
Initial vertical effective pressure (MPa)	30
Upstream pressure (MPa)	55
Downstream pressure (MPa)	54.9

rock matrix, facilitating a comparison between the numerical and analytical approaches.

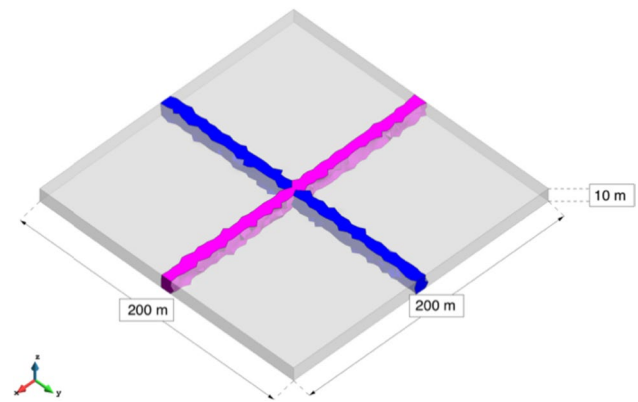
The details provided in Table 1 encompass a range of properties, including permeability and porosity of the matrix rock, as well as dimensions and initial stress states for all the analyzed scenarios.

The porosity field varies with depletion and is determined based on the volumetric deformation of the porous medium, as explained in Sect. “Update of the porosity and permeability of the fractured porous medium”. Consequently, the permeability of the rock also changes. Table 2 displays the porosity variations corresponding to the evaluated pore pressure values.

## Results

In this study, we emphasize the efficacy of the finite element method with embedded strong discontinuities for modeling discontinuities within porous media. The main objective is to demonstrate this technique as a precise and efficient alternative, especially when addressing the geomechanical behavior of naturally fractured reservoirs (NFRs) and considering the hydromechanical coupling.

To achieve this objective, four scenarios were considered for simulation. Firstly, a hypothetical scenario in line with Oda's assumptions was proposed, where fractures are interconnected and span the entire cell. This scenario was designed to validate the hydromechanical numerical model. Subsequently, three representative sections of an offshore carbonate reservoir

**Fig. 5** FEM mesh of the hypothetical scenario**Table 3** Physical parameters

Fractures	1	2
Permeability (mD)	5.3E5	5.3E5
Initial aperture (m)	8E-05	8E-05

from the pre-salt layer, explored by Petrobras in Brazil, were selected. Each section displays varying fracture frequencies and intensities. In the carbonate scenarios A, B, and C, Oda's premises, regarding the fractures being interconnected and covering the entire cell, are not valid.

## Hypothetical scenario

First, a scenario aligned with Oda's assumptions is presented, created to validate the numerical hydromechanical model. In this experiment, depicted in Fig. 5, a hypothetical reservoir with two pre-determined fractures is simulated. The main fractures within the reservoir are identified, each with identical physical parameters. It is important to note that Oda's approach assumes that all fractures are interconnected and span the entire reservoir. The reservoir itself measures 200 m × 200 m × 10 m, and the specific parameters of the fractures are outlined in Table 3.

The initial simulation was conducted at a liquid pressure of 55 MPa, with subsequent simulations decrementing the pressure in intervals of 5 MPa until a pore pressure of 10 MPa was attained. Figure 6 presents the results of these numerical analyzes, showcasing the pore pressure field, porosity field, and vertical stress field. Additionally, it details the horizontal

**Table 2** Porosity according to pore pressure

Pore Pressure (MPa)	55	50	45	40	35	30	25	20	15	10
Porosity %	7,58	7,56	7,54	7,52	7,50	7,48	7,46	7,44	7,42	7,40

direction along the "y" axis under a liquid pressure of 55 MPa with an applied pressure gradient of 0.1 MPa.

Figure 7 displays the results corresponding to the horizontal direction of the "x" axis, in continuation with those discussed previously. These data for the horizontal directions demonstrate a uniform evolution of both the pressure and stress fields.

When examining the flow direction in the horizontal orientations, it becomes apparent that the reservoir's behavior remains consistently similar. This is attributed to the pore pressure and depletion exhibiting equivalence along these directions. Such a phenomenon arises because the permeability of the rock and the fractures is identical in both horizontal directions.

To analyze the reservoir's behavior when the flow is imposed in the vertical direction, Fig. 8 shows a gradual transition in the pore pressure field, the porosity field, and the vertical stress field.

As outlined at the beginning of this section, the first scenario was designed in alignment with Oda's assumptions, wherein the fractures are interconnected and entirely span the grid cell. This setting serves as a foundation for validating the numerical hydromechanical model against Oda's proposed approach. It should be noted that, at this stage, geomechanical changes in the rock are not accounted for in the analytical solutions. To underscore the importance of integrating geomechanics into reservoir simulations, it's highlighted that as the reservoir depletes, the fracture closes, subsequently updating its aperture and, consequently, its equivalent permeability.

Figure 9 presents a comparison between the numerical and analytical solutions regarding equivalent permeability, considering flow directed in various orientations. It's paramount to emphasize that the numerical approach considers geomechanical updates of the rock, whereas the analytical

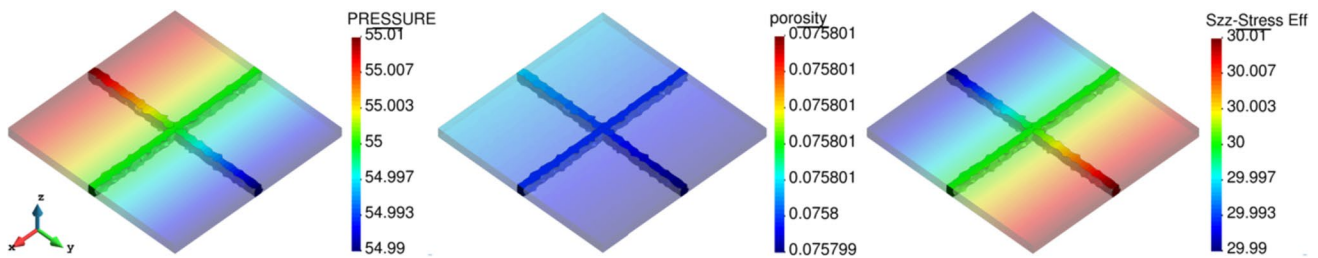


**Fig. 6** Numerical results highlighting the pore pressure field, the porosity field and the vertical stress field for the horizontal flow direction in y, in the hypothetical scenario

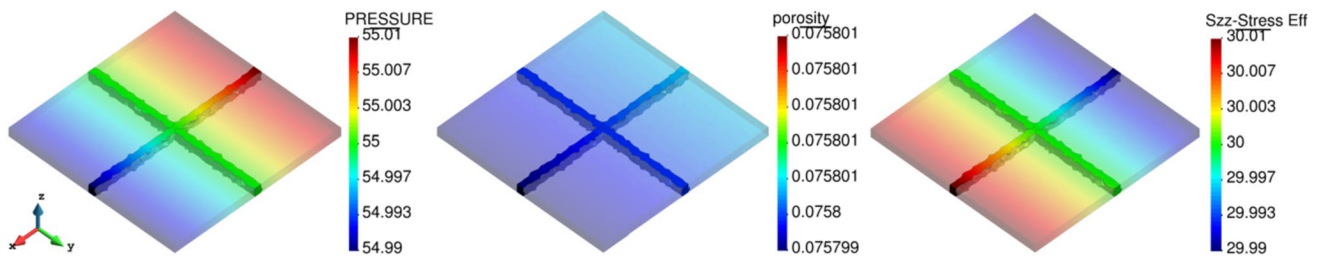


**Fig. 7** Numerical results highlighting the pore pressure field, the porosity field and the vertical stress field for the horizontal flow direction in x, in the hypothetical scenario

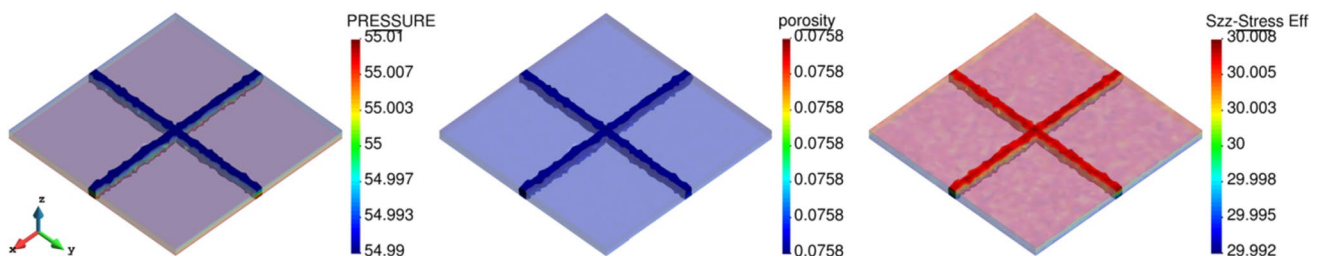


**Fig. 8** Numerical results highlighting the pore pressure field, the porosity field and the vertical stress field for the vertical flow direction, in the hypothetical scenario



**Fig. 9** Comparison between numerical and analytical equivalent permeability responses in horizontal **a** and vertical **b** flow directions in the hypothetical scenario, disregarding geomechanical aspects

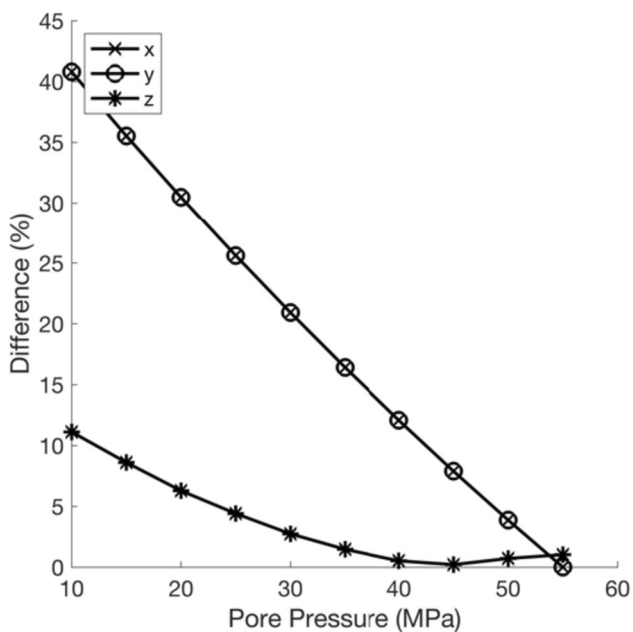
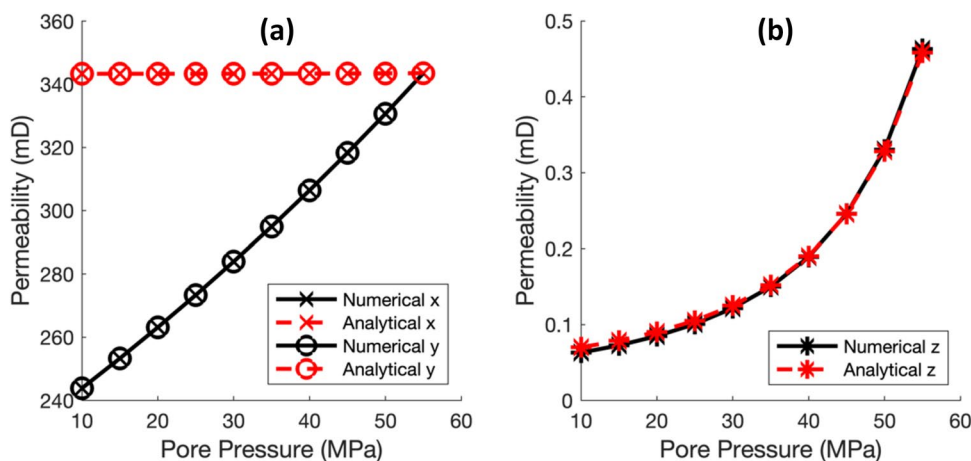


**Fig. 10** Discrepancies between numerical and analytical equivalent permeability responses in each flow direction in the hypothetical scenario, disregarding geomechanical aspects

one does not. Due to the significant disparity between the horizontal and vertical rock permeabilities, which are 343.2 mD and 0.026 mD respectively, the data was plotted on separate charts.

These results show that the analytical equivalent permeability has clearly outnumbered over the numerical equivalent permeability for both horizontal flow direction, “x” and “y”, while for the vertical flow direction, “z”, it was closer, this is due to account of the low permeability of the rock in the vertical direction, 0.026 mD, which causes the flow to occur almost exclusively through the fractures.

By comparing both results, Fig. 10 shows that there was a gap between both response, 40% and 11% for horizontal

and vertical flow direction respectively at 10 MPa of pore pressure. For 55 MPa, pore pressure for both horizontal and vertical scenarios it can be verified 0.2% and 1% of difference between the numerical and the analytical response.

It was detected that the higher the depletion, the bigger the difference between the analytical and numerical responses. However, although the gap between both numerical and analytical solutions was expected, it was noticed that a geomechanical phenomenon of updating the parent rock permeability was count by the numerical solution, while it was lost by the analytical approach. This phenomenon occurs due to pore pressure depletion, and it is calculated based on the elastic geomechanical law based on the new stress state and the consequent volumetric deformation. This calculus provides a porosity update allowing to predict the new permeability of the rock.

Thus, we incorporated into the analytical strategy an update for the matrix rock permeability. This reconfigured analytical approach unfolds in three phases: firstly, fracture openings are updated based on the Barton & Bandis method; subsequently, these updated values are employed in Oda's methodology to determine the equivalent permeability of the fracture network; finally, this equivalent permeability of the fracture network is integrated with the previously computed permeability updates for the rock matrix.

Credits to these modifications, the analytical solution aligned more accurately with the numerical responses across all flow directions, as evident in the graphs of Fig. 11.

In Fig. 12, it can be observed that the discrepancy between the numerical and analytical responses for the vertical flow direction is remarkably slight, ranging from 0.76% to 1.03%. Within the same figure, for the horizontal flow directions, this deviation is even more minimal, registering below 0.14%.

The analytical approach, by considering reservoir pressure variations and updating the fracture openings, as



**Fig. 11** Comparison between numerical and analytical equivalent permeability responses in the horizontal **a** and vertical **b** flow directions in the hypothetical scenario, considering the geomechanical aspects

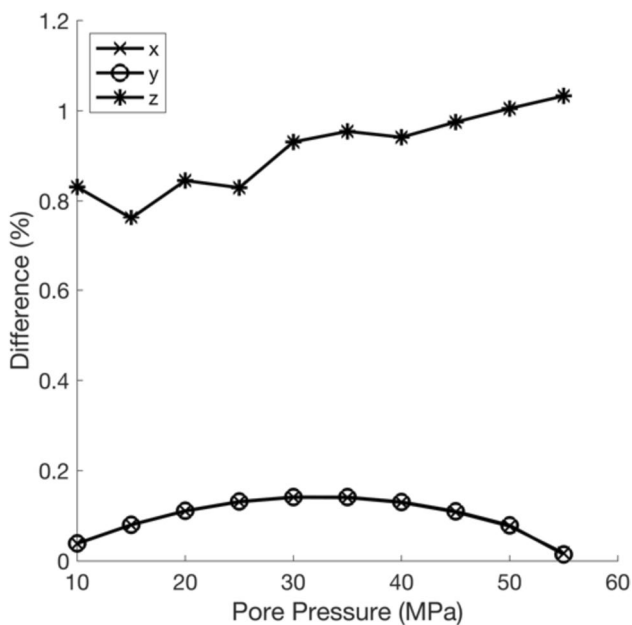
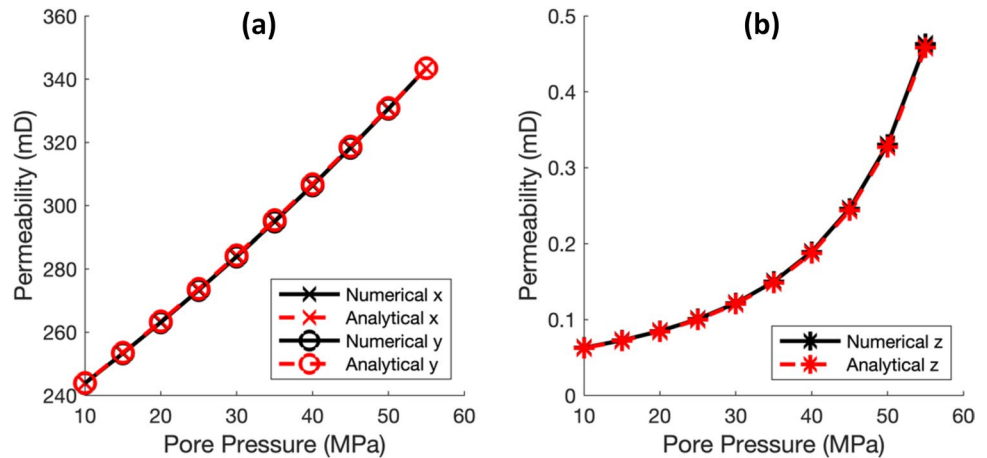


**Fig. 12** Discrepancies between numerical and analytical equivalent permeability responses in each flow direction in the hypothetical scenario, considering geomechanical aspects

well as the porosity and permeability of the rock matrix, significantly narrowed the agreement between analytical and numerical results in the given scenario.

### Carbonate reservoir scenario

The carbonate reservoir scenarios analyzed were adapted from (Falcao et al. 2018). They developed several DFN models for a carbonate reservoir in the Brazilian pre-salt interval, whose geological model built with approximately 12,000 fractures used to extract the fracture distribution examples is illustrated in Fig. 13. The Santos Basin pre-salt reservoirs are in deep waters, approximately 2,000

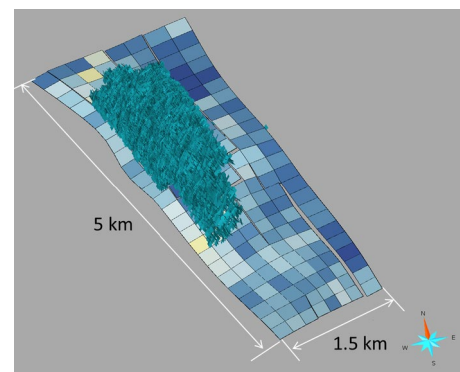


**Fig. 13** Geological model built with approximately 12,000 fractures

m and 290 km off the coast of Rio de Janeiro, which are mainly composed of carbonate rocks. Developments in these reservoirs present many challenges, due to water depth, reservoir heterogeneity and oil with  $\text{CO}_2$  content in the gaseous phase (Fraga et al. 2015).

Three DFN cells of the geological model, with dimensions of 200 m  $\times$  200 m  $\times$  10 m each, were analyzed. These three cells will represent three distinct scenarios with varying fracture intensities and densities. The scenarios will be named as carbonate reservoir A, carbonate reservoir B, and carbonate reservoir C, where the number of fractures increases in each scenario, with 26, 54, and 115 fractures, respectively. This will also assess the technique's capability to simulate DFN cells with high fracture intensity.

### Carbonate reservoir A

Figure 14 displays a 3D cell representing the first volume extracted from the geological model, predominantly containing 26 fractures oriented along the y-axis. The visualization indicates that the fractures do not span the entire length of

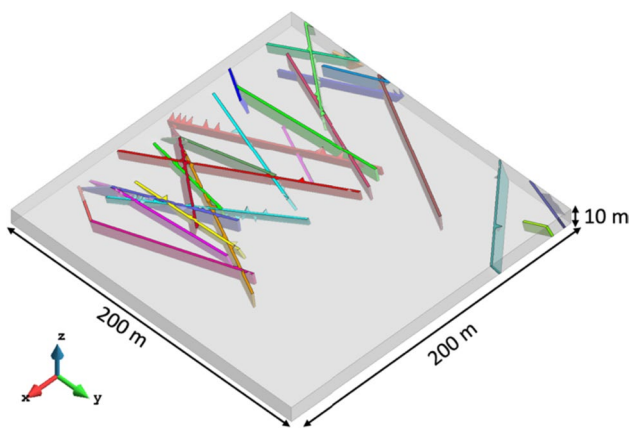


Fig. 14 MEF mesh of the carbonate reservoir A

the cell in the x and y directions, contrasting with Oda's methodology, where fractures should cover the entire cell. It's important to note that elements with fractures align with the finite element mesh. This alignment facilitates a less stringent discretization, especially in elements without fractures, making the simulation more efficient without compromising accuracy. Such strategy is applied in all studied scenarios.

The permeability details and initial apertures of the fractures for the carbonate reservoir scenario A are specified in Table 4, while the initial and boundary conditions and reservoir characteristics were discussed in the methodology section and are summarized in Table 1.

Analogous to the analyzes of the hypothetical scenario, Figs. 15 and 16 present the pore pressure, porosity and vertical stress fields at a pressure of 55 MPa, in the horizontal

Table 4 Fractures permeability and initial apertures for carbonate reservoir A

Fractures	1	2	3	4	5	6	7	8	9	10
Permeability (mD)	1,10E-01	2,40E-02	6,60E-02	7,70E-02	2,60E-02	6,00E-03	1,00E-02	3,30E-02	5,00E-03	7,20E-02
Initial aperture (m)	1,00E-05	4,69E-07	3,54E-06	4,89E-06	5,62E-07	2,81E-08	8,34E-08	9,05E-07	2,22E-08	4,29E-06
Fractures	11	12	13	14	15	16	17	18	19	20
Permeability (mD)	9,11E-01	2,00E-02	3,85E-01	1,46E-01	7,16E-01	9,70E-02	1,03E-01	8,00E-03	1,40E-02	8,00E-03
Initial aperture (m)	6,82E-04	3,28E-07	1,22E-04	1,75E-05	4,22E-04	7,73E-06	8,68E-06	5,82E-08	1,68E-07	5,56E-08
Fractures	21	22	23	24	25	26				
Permeability (mD)	2,75E-01	3,80E-02	2,20E-02	1,00E-02	2,84E-01	1,49E-01				
Initial aperture (m)	6,20E-05	1,18E-06	4,13E-07	7,55E-08	6,65E-05	1,84E-05				

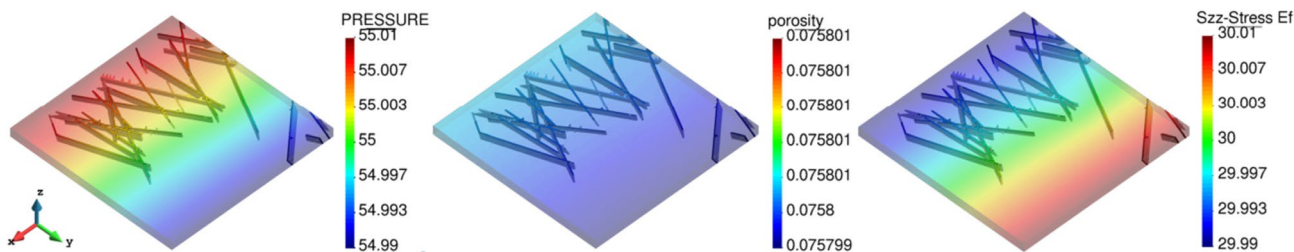


Fig. 15 Numerical results highlighting the pore pressure field, the porosity field and the vertical stress field for the horizontal flow direction in y, in the carbonate scenario A

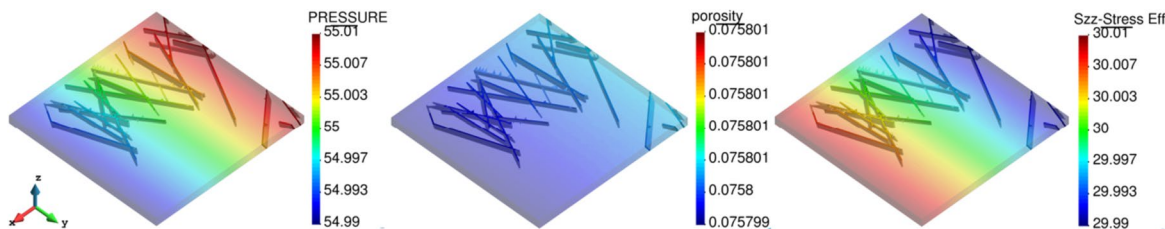
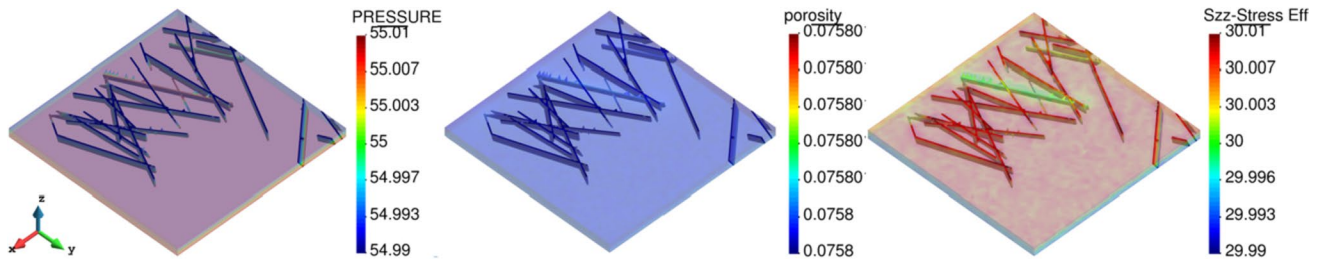
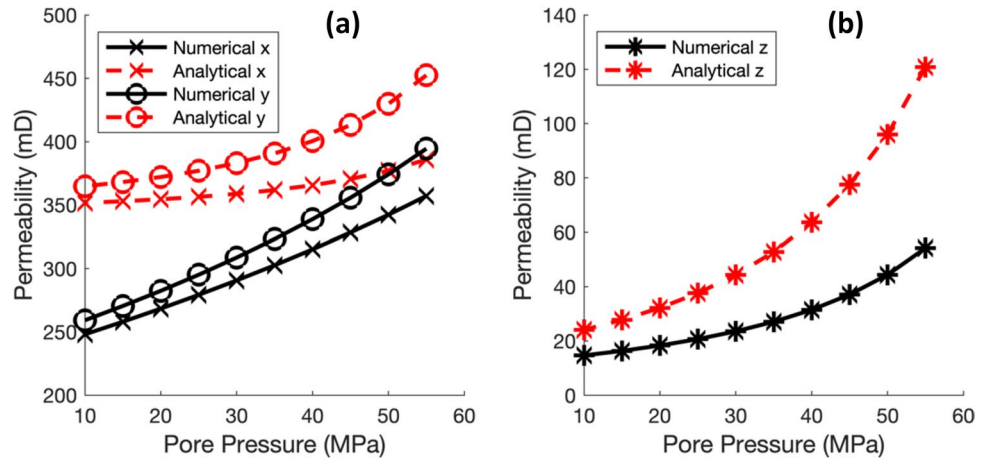


Fig. 16 Numerical results highlighting the pore pressure field, the porosity field and the vertical stress field for the horizontal flow direction in x, in the carbonate scenario A



**Fig. 17** Numerical results highlighting the pore pressure field, the porosity field and the vertical stress field for the vertical flow direction, in the carbonate scenario A

**Fig. 18** Comparison between numerical and analytical equivalent permeability responses in horizontal **a** and vertical **b** flow directions in the carbonate reservoir A, disregarding geomechanical aspects



"y" and "x" directions, respectively. Figure 17 illustrates the results for the vertical flow direction, "z".

The response of 55 MPa represents the reservoir's initial condition, which corresponds to its current state before any exploitation. Therefore, to predict the reservoir's behavior during fluid extraction, a reduction from 55 to 10 MPa was imposed, as shown in the graphs.

This study also aims to highlight the significance and impact of incorporating geomechanics into the numerical and analytical solutions concerning equivalent permeability. In this regard, Fig. 18 contrasts the numerical and analytical solutions for equivalent permeability. It is essential to emphasize that, at this stage of the analysis, the numerical solution integrates the effects of geomechanics, whereas the analytical solution does not.

Upon analyzing Fig. 19, a notable discrepancy between the result sets is observed. For a flow in the horizontal direction and a pore pressure of 10 MPa, the divergence between the numerical and analytical solutions exceeds 40%. However, this difference tends to decrease as the fractures open, reaching variations between 8 and 14% at a pore pressure of 55 MPa, for flow directions in x and y, respectively. In the vertical flow, the discrepancy is even more pronounced. At 10 MPa of pore pressure, the difference surpasses 64%, and this margin increases as the

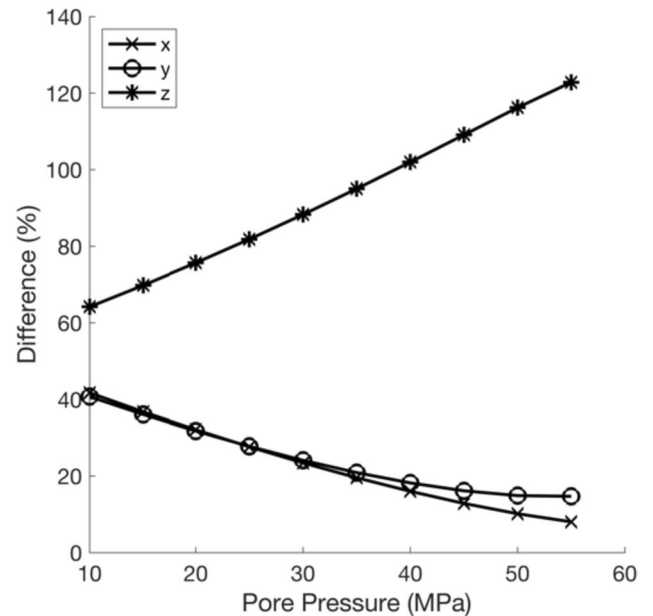
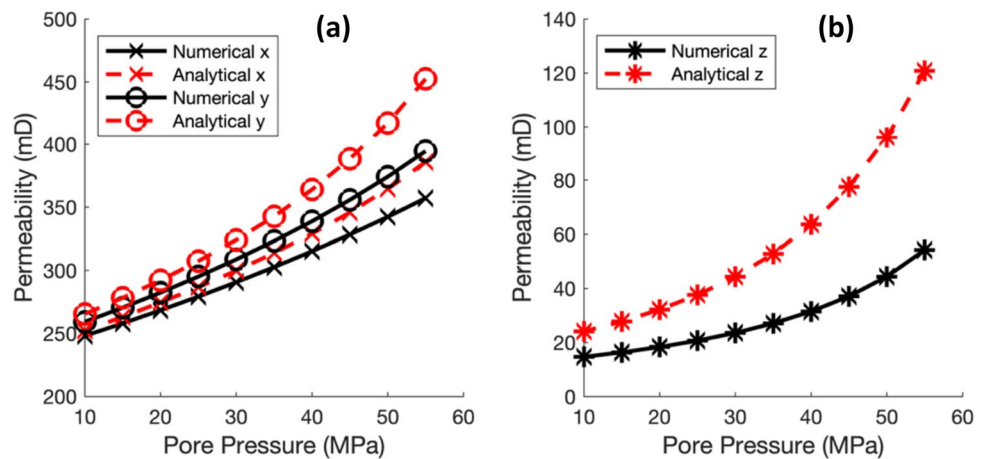


**Fig. 19** Discrepancies between numerical and analytical equivalent permeability responses in each flow direction in the carbonate reservoir A, disregarding geomechanical aspects

**Fig. 20** Comparison between numerical and analytical equivalent permeability responses in horizontal **a** and vertical **b** flow directions in the carbonate reservoir A, considering geomechanical aspects



fractures become more open, even exceeding 120% at 55 MPa.

Figure 20 presents a comparison of the equivalent permeability between the numerical and analytical results, considering the geomechanical effects in both approaches. These effects are primarily manifested in the changes in fracture apertures and in variations of porosity and permeability of the matrix rock. It was considered that the update of the matrix rock permeability was consistent between the two approaches. Thus, any discrepancies between the results mainly arise from how each method addresses the flow within the fractures.

The analysis indicates that as depletion progresses and the fractures close further, the agreement between the two approaches intensifies. This reinforces the idea that the equivalent permeability becomes increasingly influenced by the intrinsic permeability of the matrix rock.

As depletion intensifies, analytical and numerical solutions converge. The difference between them is most pronounced in the vertical flow direction. In the vertical direction, discrepancies remain consistent with those obtained without considering geomechanical factors. This is because the permeability of the rock matrix in this direction is quite low, registering at 0.026 mD. This flow direction is heavily influenced by fractures, with 22 fractures crossing the cell in this direction. On the other hand, in horizontal directions, these differences are almost negligible. Figure 21 delves deeper into this observation, highlighting the variations between analytical and numerical approaches. With a pore pressure of 55 MPa, discrepancies in horizontal solutions range between 8 and 14% for flow directions x and y, respectively. However, when reducing the pore pressure to 10 MPa—as fractures close—the difference in horizontal directions decreases, reaching about 2% for both x and y directions.

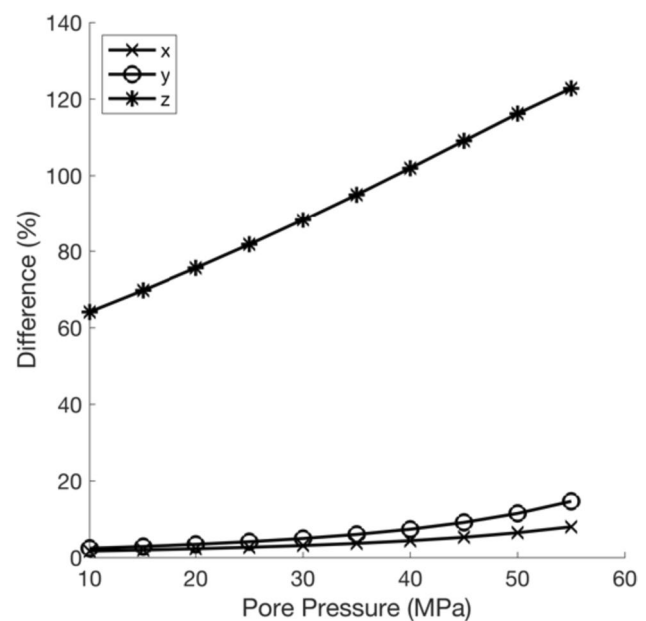


**Fig. 21** Discrepancies between numerical and analytical equivalent permeability responses in each flow direction in the carbonate reservoir A, considering geomechanical aspects

### Carbonate reservoir B

Figure 22 showcases a 3D cell depicting the second volume extracted from the geological model, referred to as the carbonate reservoir B. Within this cell, there are 54 fractures, with their aperture and permeability details outlined in Table 5. While the fractures don't span the full length of the cell, they exhibit strong connectivity, particularly along the y-axis.

Similar to the analyzes of carbonate reservoir A, Figs. 23 and 24 present the pore pressure, porosity and vertical stress fields at a pressure of 55 MPa, for carbonate reservoir B, in



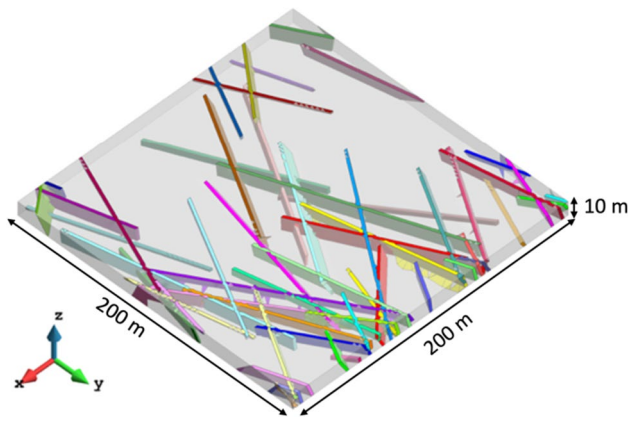


Fig. 22 MEF mesh of the carbonate reservoir B

the horizontal "y" and "x" directions, respectively. Figure 25 highlights the results in the vertical flow direction, "z".

It can be observed that with a pressure gradient depletion of 0.02 MPa, the pore pressure, vertical stress, and porosity undergo minimal changes. This subtle shift in porosity does not significantly impact the permeability of the medium. Figure 26 contrasts the update of the equivalent permeability for both the numerical and analytical solutions. It's important to note that, at this stage of the analysis, the numerical solution incorporates geomechanical effects, whereas the analytical solution does not.

When comparing the two sets of results, Fig. 27 reveals a discrepancy between the responses. In the case of horizontal flow direction, at 10 MPa of pore pressure, the difference between the numerical and analytical solutions exceeds 40%, while this gap is close to 18% and 30% at 55 MPa pore pressure. In vertical flow direction, a difference between the numerical and analytical responses can also be observed, ranging from 3.8% to 7.6% at 10 MPa and 55 MPa in pore pressure, respectively.

Table 5 Fractures permeability and initial apertures for carbonate reservoir B

Fractures	1	2	3	4	5	6	7	8	9	10
Permeability (mD)	1,00E-03	8,00E-02	7,80E-02	1,28E-01	2,00E-03	2,00E-03	4,50E-02	1,79E-01	4,69E-01	8,80E-02
Initial aperture (m)	1,07E-09	5,21E-06	4,97E-06	1,36E-05	3,45E-09	2,98E-09	1,65E-06	2,63E-05	1,81E-04	6,41E-06
Fractures	11	12	13	14	15	16	17	18	19	20
Permeability (mD)	6,00E-02	5,30E-01	6,40E-02	4,09E-01	2,00E-02	7,00E-03	4,60E-02	1,45E-04	9,14E-01	6,00E-02
Initial aperture (m)	2,93E-06	2,31E-04	3,38E-06	1,37E-04	3,18E-07	4,47E-08	1,73E-06	1,76E-11	6,87E-04	3,00E-06
Fractures	21	22	23	24	25	26	27	28	29	30
Permeability (mD)	1,70E-02	1,99E-01	1,00E-03	2,70E-02	6,00E-03	9,30E-02	2,00E-03	1,51E-01	7,02E-01	1,00E-03
Initial aperture (m)	2,41E-07	3,25E-05	1,40E-09	5,99E-07	2,57E-08	7,08E-06	2,45E-09	1,87E-05	4,06E-04	1,02E-09
Fractures	31	32	33	34	35	36	37	38	39	40
Permeability (mD)	1,00E-03	4,00E-03	2,00E-03	1,19E-01	2,16E-01	2,80E-02	4,80E-02	3,93E-01	1,23E-01	1,70E-02
Initial aperture (m)	5,38E-10	1,30E-08	2,10E-09	1,16E-05	3,84E-05	6,26E-07	1,86E-06	1,27E-04	1,24E-05	2,46E-07
Fractures	41	42	43	44	45	46	47	48	49	50
Permeability (mD)	4,40E-02	9,60E-01	1,65E-01	5,14E-01	1,43E-01	2,20E-02	1,80E-02	2,50E-02	1,80E-02	2,40E-02
Initial aperture (m)	1,59E-06	7,57E-04	2,23E-05	2,17E-04	1,68E-05	3,89E-07	2,76E-07	5,17E-07	2,72E-07	4,76E-07
Fractures	51	52	53	54						
Permeability (mD)	1,33E-01	5,50E-02	6,80E-02	4,00E-03						
Initial aperture (m)	1,46E-05	2,53E-06	3,76E-06	1,11E-08						

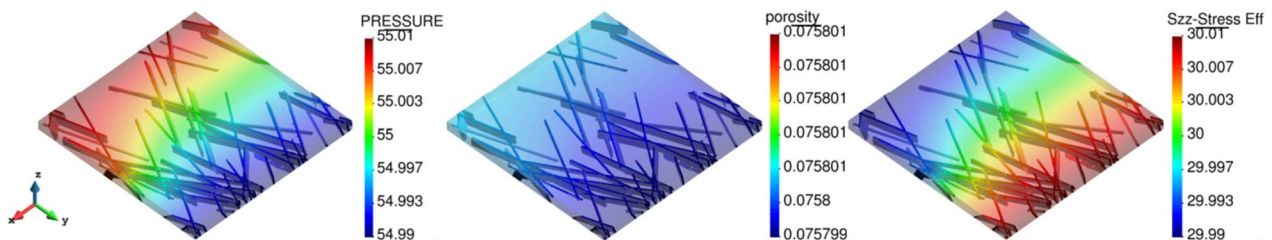
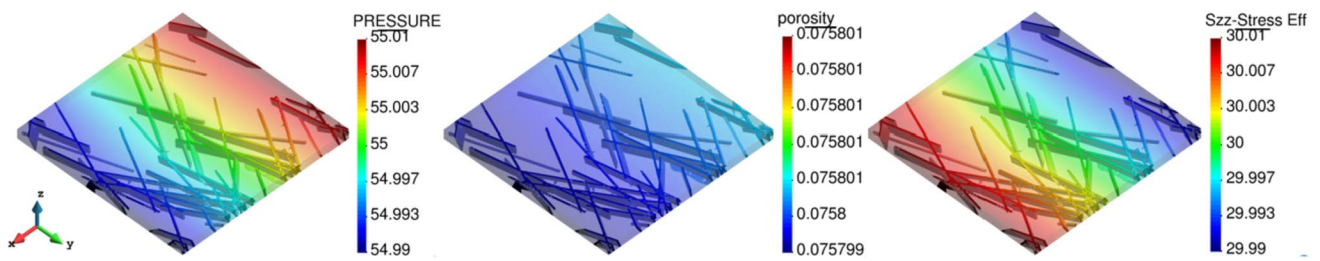
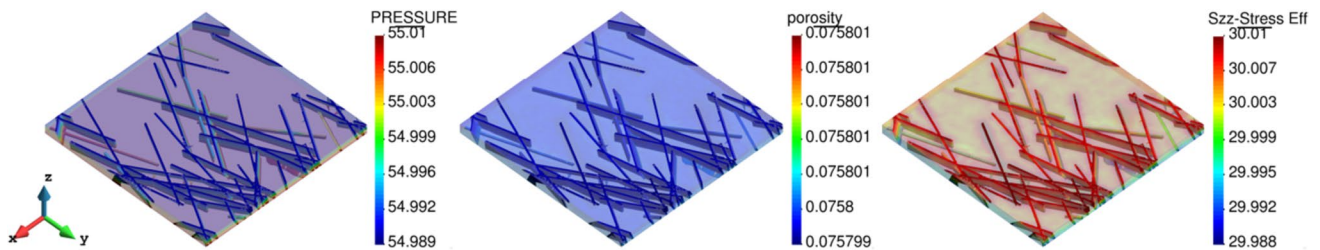


Fig. 23 Numerical results highlighting the pore pressure field, the porosity field and the vertical stress field for the horizontal flow direction in y, in the carbonate scenario B





**Fig. 24** Numerical results highlighting the pore pressure field, the porosity field and the vertical stress field for the horizontal flow direction in *x*, in the carbonate scenario B



**Fig. 25** Numerical results highlighting the pore pressure field, the porosity field and the vertical stress field for the vertical flow direction, in the carbonate scenario B

**Fig. 26** Comparison between numerical and analytical equivalent permeability responses in horizontal **a** and vertical **b** flow directions in the carbonate reservoir B, disregarding geomechanical aspects

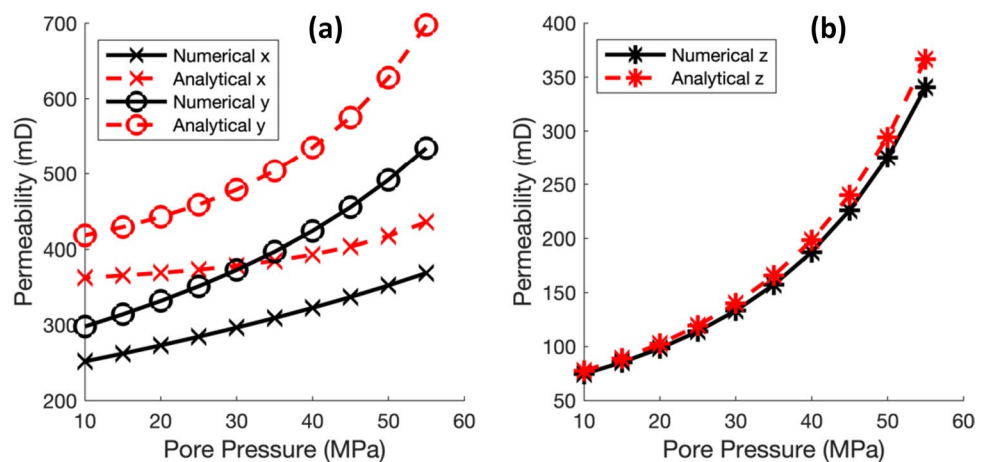
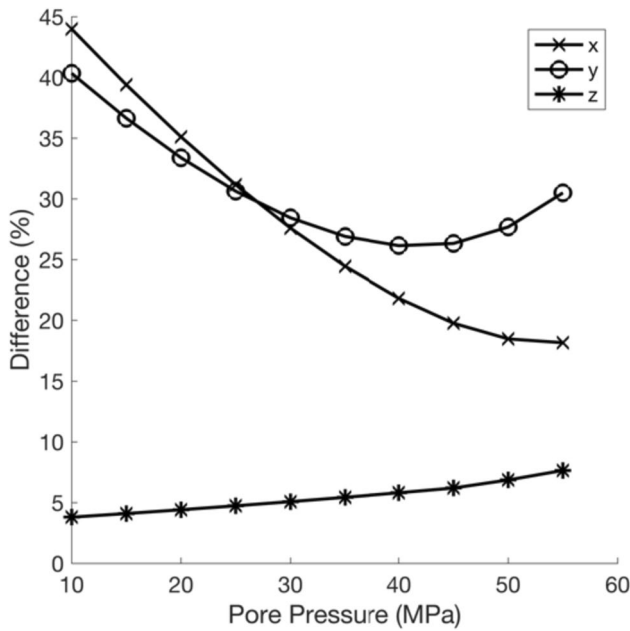


Figure 28 compares the equivalent permeability for the scenario of the carbonate reservoir B, using both numerical and analytical results, with both considering the geomechanical effects. Just as observed in the scenario of the carbonate reservoir A, as the depletion intensifies and the fractures begin to close, the flow is progressively more influenced by the matrix rock. Consequently, the agreement between both approaches strengthens.

These results indicate that as the depletion increases, the analytical and numerical solutions become closer. Notably, the discrepancies between the two solutions are more pronounced in the horizontal flow directions, while the results for the vertical flow direction show minimal differences. This

observation is further highlighted in Fig. 22, which illustrates the inaccuracies between the analytical and numerical solutions. At a pore pressure of 50 MPa, the differences between the solutions amount to approximately 18.2% for the "x" direction, 30.5% for the "y" direction, and 7.6% for the "z" direction. In contrast, at a pore pressure of 10 MPa, corresponding to a depletion of 45 MPa, the discrepancies reduce to approximately 4.6% for the "x" direction, 7.0% for the "y" direction, and 3.8% for the "z" direction (Fig. 29).



**Fig. 27** Discrepancies between numerical and analytical equivalent permeability responses in each flow direction in the carbonate reservoir B, disregarding geomechanical aspects

**Carbonate reservoir C**

The 3D cell depicted in Fig. 30 displays the third volume extracted from the geological model, pertaining to the carbonate reservoir scenario C. This cell contains 115 fractures, highlighting the capability of the embedded strong discontinuities technique to represent a DFN with greater fracture frequency and intensity. The aperture and permeability of these fractures are detailed in Table 6. Although the fractures do not span the entire length of the cell in the

x and y directions, the image shows a notable connectivity between them.

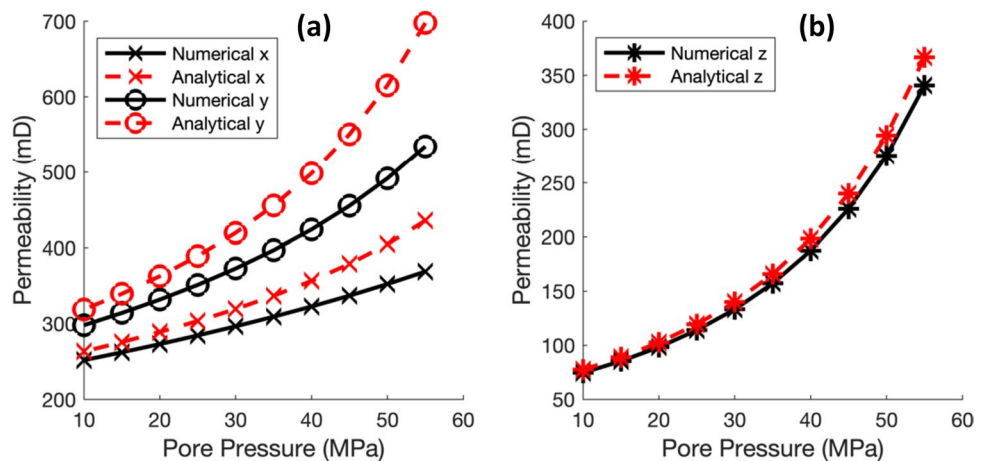
Similar to previous analyzes, Figs. 31 and 32 present the pore pressure, porosity and vertical stress fields at a pressure of 55 MPa, in the horizontal "y" and "x" directions, respectively. Figure 33 highlights the results in the vertical flow direction, "z".

Just like in previous cases, it's noticeable that with a pressure gradient depletion of 0.02 MPa, the variations in pore pressure, vertical stress, and porosity are minimal. This subtle change in porosity has a limited impact on the permeability of the medium. Figure 34 compares the update of the equivalent permeability in the scenario of the carbonate reservoir C, addressing both numerical and analytical solutions. Once again, it is observed that the analytical solution tends to overestimate the equivalent permeability.

Upon examining the two sets of results depicted in Fig. 35, a notable discrepancy between the responses is evident. For the horizontal flow in the x direction, at a pore pressure of 10 MPa, the variation between the numerical and analytical solutions exceeds 48%. This variation slightly decreases to about 35% at 40 MPa and then rises again, surpassing 42% when the pore pressure reaches 55 MPa. On the other hand, in the y direction of the flow, the difference between solutions exceeds 43% at 10 MPa, slightly decreases to 39% at 30 MPa, and subsequently ascends to over 63% at 55 MPa of pore pressure. In the vertical flow, the presence of a significant number of fractures intersecting the cell and the reduced permeability of the rock matrix in that direction ensure that flow predominantly occurs through the fractures. The discrepancies between the numerical and analytical solutions remain relatively stable, fluctuating around 7% to 8% for pore pressures of 10 MPa and 55 MPa, respectively.

Figure 36 compares the equivalent permeability for the carbonate reservoir C scenario, using numerical and analytical results, both considering geomechanical effects. When taking geomechanical aspects into account, updates

**Fig. 28** Comparison between numerical and analytical equivalent permeability responses in horizontal **a** and vertical **b** flow directions in the carbonate reservoir B, considering geomechanical aspects



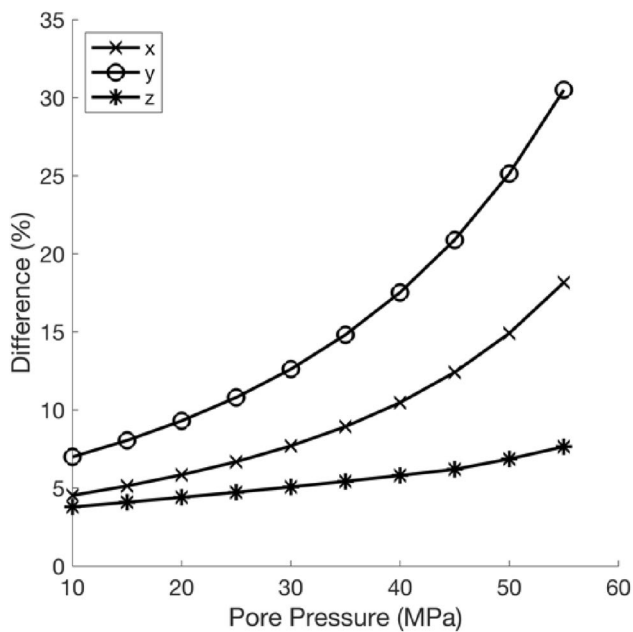


**Fig. 29** Discrepancies between numerical and analytical equivalent permeability responses in each flow direction in the carbonate reservoir B, considering geomechanical aspects

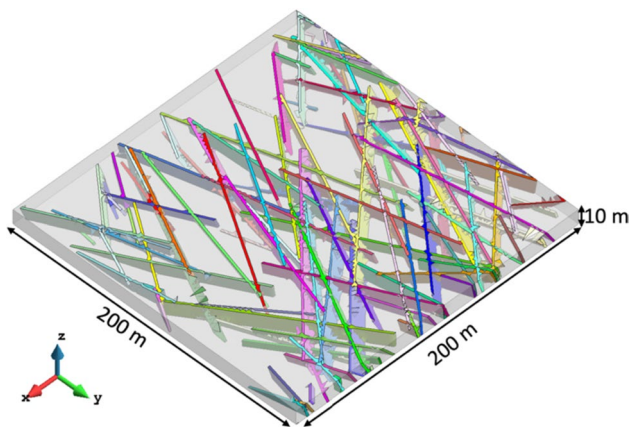


**Fig. 30** MEF mesh of the carbonate reservoir C

in fracture openings, as well as in the permeability and porosity of the rock matrix, become evident. The results suggest that as depletion intensifies, the fractures tend to close. This causes the flow to become less dependent on them, thereby bringing the analytical and numerical solutions closer together.

Figure 37 highlights the differences between analytical and numerical solutions for the equivalent permeability in the context of carbonate reservoir C, considering geomechanical updates. The graph reveals that discrepancies between both solutions are more pronounced in horizontal flow directions, especially when the flow occurs in the

y-direction, which corresponds to the main direction of the fractures. At a pore pressure of 10 MPa, the variations between the solutions reach 11% in the x-direction and 14% in the y-direction. In contrast, under a pore pressure of 55 MPa, these discrepancies increase significantly, reaching 42% in the x-direction and exceeding 63% in the y-direction. Meanwhile, results in the vertical flow direction remain stable, fluctuating between 7 and 8%.

## Discussion

### Geomechanical effects in NFRs equivalent permeability

The initial scenario, aligned with Oda's assumptions, in which fractures are interconnected and span the entire grid cell, was designed to ensure no differences between numerical and analytical results. With this strategy, it was managed to emphasize the significance of integrating geomechanical effects and validate the use of the embedded strong discontinuity approach in the analysis of equivalent permeability in NFRs.

However, in the initial approach where the analytical solution does not take geomechanical effects into account, a discrepancy between the results becomes apparent, indicating the need for modifications in the analytical approach.

Upon investigating the root of this misalignment, it was discerned that the distinction between numerical and analytical approaches lay in the considerations of geomechanical effects. This allowed for a narrowing of the gap between the results.

As a result, the maximum difference between the two solutions significantly decreased. The initial discrepancy of 40% in the horizontal flow direction was reduced to less than 0.14%, while in the vertical direction, it diminished from 11% to a peak of 1.03%.

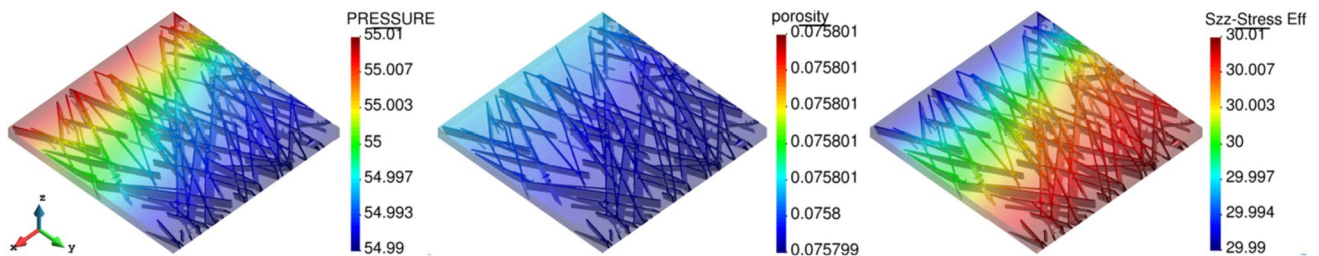
Consequently, these findings validated the use of the embedded strong discontinuity technique and underscore the importance of incorporating geomechanical effects in the analysis of equivalent permeability in NFRs.

### Embedded strong discontinuity technique in the analysis of NFRs equivalent permeability

While the embedded strong discontinuity technique has been shown to be a precise alternative for modeling discontinuities in porous media, like in NFRs, it's essential to determine the specific advantages or conditions that would justify choosing the numerical approach over the analytical one, particularly when considering geomechanical effects.

**Table 6** Fractures permeability and initial apertures for carbonate reservoir C

Fractures	1	2	3	4	5	6	7	8	9	10
Permeability (mD)	3.57E-06	8.80E-11	2.32E-10	1.26E-05	2.65E-07	1.22E-05	5.03E-07	3.53E-04	1.02E-07	5.01E-09
Initial aperture (m)	6.60E-02	3.25E-04	1.00E-03	1.24E-01	1.80E-02	1.22E-01	2.50E-02	6.55E-01	1.10E-02	2.00E-03
Fractures	11	12	13	14	15	16	17	18	19	20
Permeability (mD)	2.78E-07	9.32E-09	3.84E-10	1.26E-07	2.07E-05	1.39E-08	6.12E-04	2.07E-08	7.02E-08	1.24E-08
Initial aperture (m)	1.80E-02	3.00E-03	1.00E-03	1.20E-02	1.59E-01	4.00E-03	8.63E-01	5.00E-03	9.00E-03	4.00E-03
Fractures	21	22	23	24	25	26	27	28	29	30
Permeability (mD)	2.57E-04	2.24E-04	3.21E-04	1.68E-05	1.63E-06	2.68E-05	2.60E-04	2.21E-07	4.20E-07	4.39E-07
Initial aperture (m)	5.59E-01	5.22E-01	6.25E-01	1.43E-01	4.50E-02	1.81E-01	5.62E-01	1.60E-02	2.30E-02	2.30E-02
Fractures	31	32	33	34	35	36	37	38	39	40
Permeability (mD)	3.29E-08	1.93E-08	7.96E-09	1.17E-06	3.58E-05	1.18E-05	5.30E-05	7.01E-05	4.61E-06	7.09E-06
Initial aperture (m)	6.00E-03	5.00E-03	3.00E-03	3.80E-02	2.09E-01	1.20E-01	2.54E-01	2.92E-01	7.50E-02	9.30E-02
Fractures	41	42	43	44	45	46	47	48	49	50
Permeability (mD)	4.60E-09	3.63E-04	3.40E-07	1.05E-06	1.55E-06	2.32E-05	1.21E-06	8.39E-07	1.02E-08	4.15E-04
Initial aperture (m)	2.00E-03	6.65E-01	2.00E-02	3.60E-02	4.30E-02	1.68E-01	3.80E-02	3.20E-02	4.00E-03	7.10E-01
Fractures	51	52	53	54	55	56	57	58	59	60
Permeability (mD)	1.92E-04	1.83E-07	2.07E-06	1.83E-07	8.08E-04	1.26E-06	6.10E-05	7.72E-08	3.63E-08	9.00E-08
Initial aperture (m)	4.83E-01	1.50E-02	5.00E-02	1.50E-02	9.91E-01	3.90E-02	2.72E-01	1.00E-02	7.00E-03	1.00E-02
Fractures	61	62	63	64	65	66	67	68	69	70
Permeability (mD)	3.91E-06	1.63E-05	7.64E-04	3.35E-07	3.56E-05	6.88E-05	3.62E-10	1.93E-07	4.27E-04	1.36E-05
Initial aperture (m)	6.90E-02	1.41E-01	9.64E-01	2.00E-02	2.08E-01	2.89E-01	1.00E-03	1.50E-02	7.21E-01	1.29E-01
Fractures	71	72	73	74	75	76	77	78	79	80
Permeability (mD)	4.05E-04	1.42E-07	1.72E-09	1.97E-05	4.12E-04	2.04E-08	5.57E-05	1.34E-10	8.90E-05	6.24E-04
Initial aperture (m)	7.02E-01	1.30E-02	1.00E-03	1.55E-01	7.08E-01	5.00E-03	2.60E-01	4.01E-04	3.29E-01	8.71E-01
Fractures	81	82	83	84	85	86	87	88	89	90
Permeability (mD)	2.43E-05	4.13E-06	8.82E-06	3.97E-06	1.20E-06	1.35E-06	2.34E-06	3.13E-09	1.66E-06	1.03E-05
Initial aperture (m)	1.72E-01	7.10E-02	1.04E-01	6.90E-02	3.80E-02	4.10E-02	5.30E-02	2.00E-03	4.50E-02	1.12E-01
Fractures	91	92	93	94	95	96	97	98	99	100
Permeability (mD)	1.14E-07	7.21E-10	5.17E-08	6.58E-09	7.10E-07	6.83E-05	4.04E-08	6.14E-06	4.12E-09	3.00E-06
Initial aperture (m)	1.20E-02	1.00E-03	8.00E-03	3.00E-03	2.90E-02	2.88E-01	7.00E-03	8.60E-02	2.00E-03	6.00E-02
Fractures	101	102	103	104	105	106	107	108	109	110
Permeability (mD)	2.81E-04	6.53E-10	1.23E-05	2.50E-05	4.68E-08	1.09E-04	8.76E-06	2.28E-06	3.34E-04	6.98E-04
Initial aperture (m)	5.84E-01	1.00E-03	1.22E-01	1.74E-01	8.00E-03	3.63E-01	1.03E-01	5.30E-02	6.37E-01	9.21E-01
Fractures	111	112	113	114	115					
Permeability (mD)	5.62E-06	3.43E-07	3.67E-09	5.89E-06	8.32E-09					
Initial aperture (m)	8.30E-02	2.00E-02	2.00E-03	8.50E-02	3.00E-03					

**Fig. 31** Numerical results highlighting the pore pressure field, the porosity field and the vertical stress field for the horizontal flow direction in  $y$ , in the carbonate scenario C



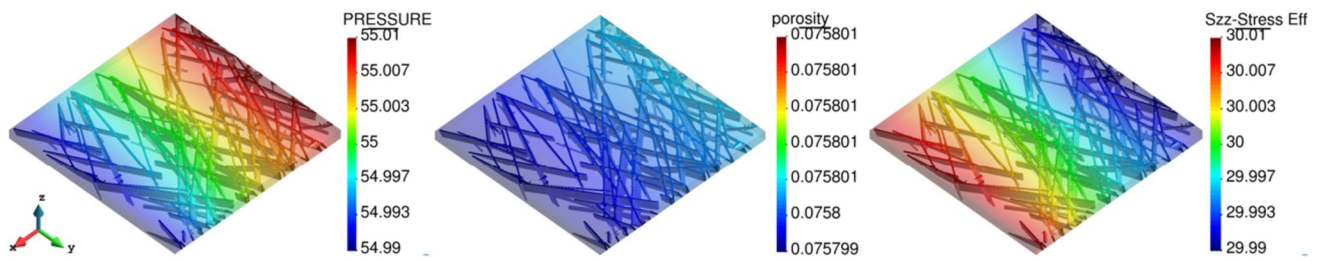


**Fig. 32** Numerical results highlighting the pore pressure field, the porosity field and the vertical stress field for the horizontal flow direction in x, in the carbonate scenario C

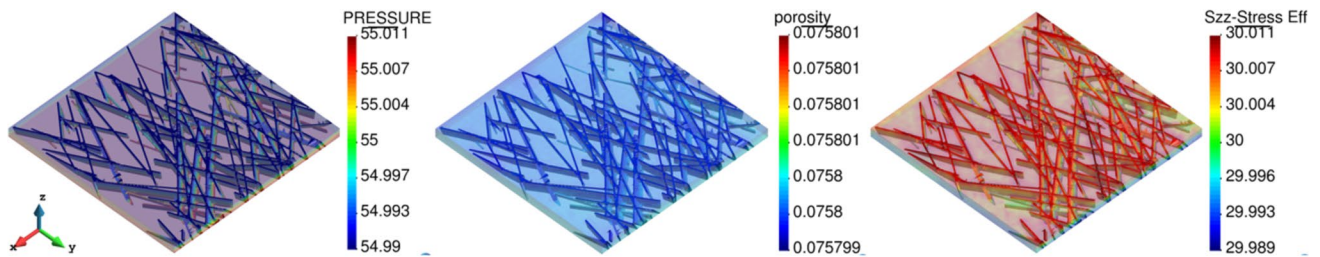
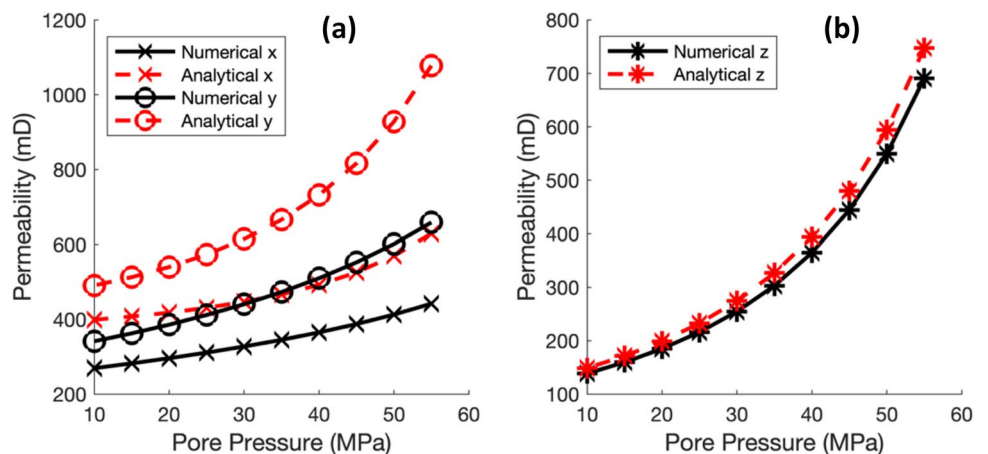


**Fig. 33** Numerical results highlighting the pore pressure field, the porosity field and the vertical stress field for the vertical flow direction, in the carbonate scenario C

**Fig. 34** Comparison between numerical and analytical equivalent permeability responses in horizontal **a** and vertical **b** flow directions in the carbonate reservoir C, disregarding geomechanical aspects



This decision becomes even more critical when considering that the analytical approach requires significantly less computational time.

Given this scenario, to clarify these uncertainties, it was considered to conduct comparisons using more realistic settings, extracted from a representative geological model of an offshore carbonate reservoir from the Brazilian pre-salt layer, investigated by Petrobras. In this context, Oda's assumptions regarding interconnected fractures that span the entire grid cell are not met.

The results showed that the analytical approach overestimates the numerical one, especially when the fractures are not well connected and cover the entire grid cell. This observation aligns with the findings of many

researchers who identified that Oda's methodology tends to overestimate the permeability of the fracture network, as reported by Dershowitz et al. (2000), Gupta et al. (2001), Decroux and Gosselin (2013), Ghahfarokhi (2017), Haridy et al. (2019), and Alvarez et al. (2021).

When contrasting the numerical and analytical approaches, it becomes apparent that the numerical tends to be more appropriate in contexts where fractures are not fully connected, especially when they do not occupy the entire grid cell. Observing the results of the carbonate scenarios:

- In carbonate reservoir A, with only 26 fractures predominantly concentrated on one side of the reservoir, the overestimation of vertical permeability was



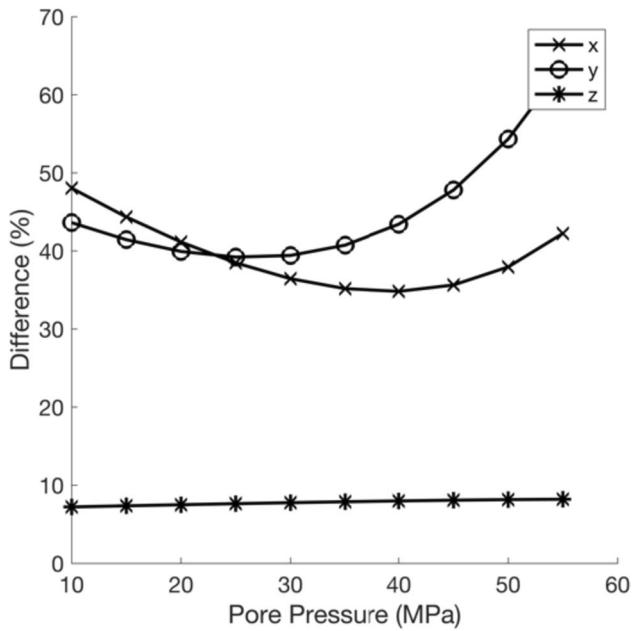


**Fig. 35** Discrepancies between numerical and analytical equivalent permeability responses in each flow direction in the carbonate reservoir C, disregarding geomechanical aspect

pronounced. This is largely due to the strong influence of the fractures and the low vertical permeability of the rock matrix.

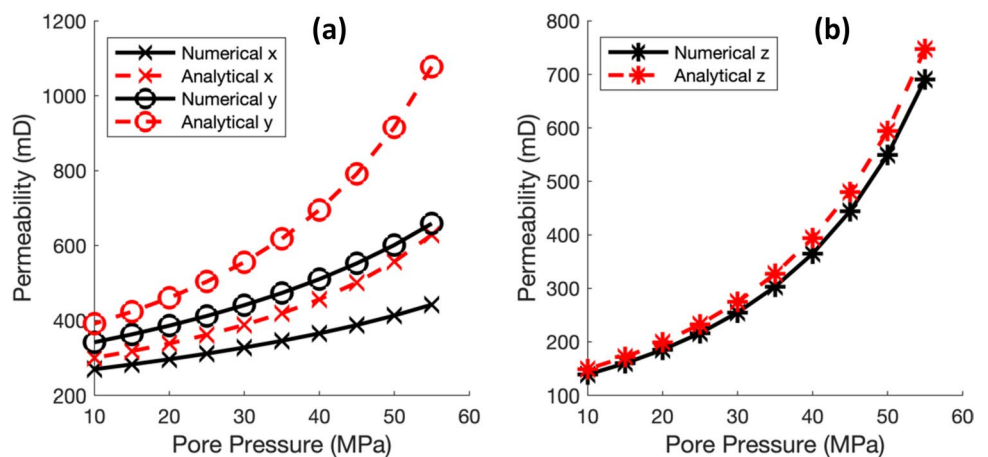
- In carbonate reservoir B, which has 54 well-connected fractures distributed throughout the cell, the fractures play a crucial role in directing the vertical flow due to the low permeability of the rock matrix. The difference between the numerical and analytical solutions is minimal in this direction. However, in the horizontal direction, the analytical solution tends to overestimate, especially in the y direction, which aligns with the main direction of the fractures.
- For carbonate reservoir C, with 115 well-distributed and connected fractures but not covering the entire cell,

the capability of the embedded strong discontinuities technique in simulating contexts with high density and intensity of fractures was emphasized. The results are similar to reservoir B, with fractures dominating the vertical flow and a notable overestimation in the horizontal direction, especially in the y direction.

For the reservoir engineer, it may be impractical to incorporate geomechanics into everyday life, given the volume of simulations required to adjust and predict different scenarios. Therefore, when determining the conditions that justify a preference for the numerical approach over the analytical one, it is essential to consider the connectivity, distribution, and density of fractures, the permeability of the rock matrix, and the flow direction. This ensures that the chosen technique is appropriate and provides reliable results. Let's examine each aspect:

- *Fracture connectivity*: Situations where fractures are not fully connected might not be ideal for the analytical approach.
- *Fracture distribution*: The location and distribution of fractures have a significant impact on the results, such as when there's a concentration of fractures in a specific part of the reservoir.
- *Rock matrix permeability*: The influence of fractures on flow can change depending on the permeability of the rock matrix. In contexts where this permeability is reduced, fractures tend to play a dominant role in the flow.
- *Flow direction*: The analytical approach often overestimates the flow, especially in the predominant direction of the fractures.
- *Fracture density and intensity*: In scenarios with high fracture density and intensity, as observed in the carbonate reservoir C, the embedded strong discontinuity technique proved valuable, suggesting that the analytical approach might not be best suited for such contexts.

**Fig. 36** Comparison between numerical and analytical equivalent permeability responses in horizontal **a** and vertical **b** flow directions in the carbonate reservoir C, considering geomechanical aspects



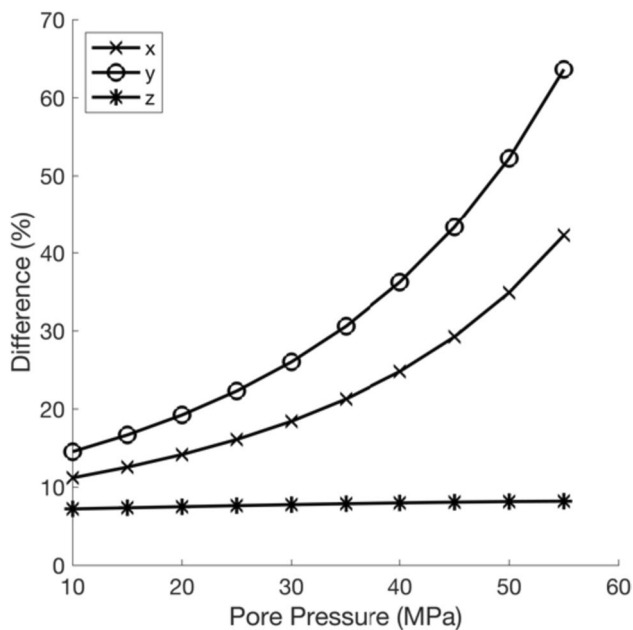


**Fig. 37** Discrepancies between numerical and analytical equivalent permeability responses in each flow direction in the carbonate reservoir C, considering geomechanical aspects

## Conclusions

The study conducted in this article employed the embedded strong discontinuities approach to explore permeability in naturally fractured reservoirs, focusing on the interplay between variable reservoir pressures and their consequences on rock porosity and permeability. From the hydromechanical simulations conducted, several important findings emerged, outlining both challenges and opportunities in modeling naturally fractured reservoirs. These findings are summarized in the following key conclusions:

- *Application of the embedded strong discontinuities approach:* Demonstrated effectiveness in determining the equivalent permeability in naturally fractured reservoirs, incorporating essential geomechanical effects.
- *Importance of geomechanics in simulations of naturally fractured reservoirs:* Pressure variations in reservoirs significantly influence fracture opening and the properties of the matrix rock, such as porosity and permeability.
- *Discrepancies between numerical and analytical solutions:* Overlooking geomechanical behavior leads to notable differences, highlighting the need for geomechanical updates for accurate permeability assessments.
- *Preference for numerical modeling in naturally fractured reservoirs:* It was observed that analytical approaches tend to overestimate the permeability of the fracture

network, especially in situations where fractures are not well connected and do not fully cross the cell.

- *Efficiency of the embedded strong discontinuities approach:* Although not faster than analytical approaches, this technique proved efficient for numerical simulations in NFRs (Naturally Fractured Reservoirs), particularly in scenarios with high fracture intensity. It balances modeling complexity with computational time efficiency.
- *Drastic reduction in the need for interface elements:* This results in a more efficient computational model, facilitating simulations and assessment of various scenarios with different fracture frequencies and intensities.
- *Perspectives for future research:* It is essential to expand research to cover various scenarios, analyzing how the frequency and intensity of fractures affect permeability. This will help identify the most effective approaches for each specific context.

**Acknowledgements** This work was conducted with the financial support of Energi Simulation and Petrobras S/A. The authors are grateful for the support of the Center of Research Leopoldo Américo Miguez de Mello (CENPES-PETROBRAS/Brazil) and the Research Group in Computational Methods in Geomechanics (LMCG-UFPE/Brazil).

**Funding** This study was funded by Petrobras and Energi Simulation.

## Declarations

**Conflict of interest** On behalf of all authors, the corresponding author states that there is no conflict of interest.

**Open Access** This article is licensed under a Creative Commons Attribution 4.0 International License, which permits use, sharing, adaptation, distribution and reproduction in any medium or format, as long as you give appropriate credit to the original author(s) and the source, provide a link to the Creative Commons licence, and indicate if changes were made. The images or other third party material in this article are included in the article's Creative Commons licence, unless indicated otherwise in a credit line to the material. If material is not included in the article's Creative Commons licence and your intended use is not permitted by statutory regulation or exceeds the permitted use, you will need to obtain permission directly from the copyright holder. To view a copy of this licence, visit <http://creativecommons.org/licenses/by/4.0/>.

## References

- Ahmed M (2014) Improved upscaling and reservoir simulation of enhanced oil recovery processes in naturally fractured reservoirs. Doctoral Dissertation, Heriot-Watt University.
- Alvarez L, Guimarães L, Gomes I, Beserra L, Pereira L, Miranda T, Maciel B, Barbosa A (2021) Impact of fracture topology on the fluid flow behavior of naturally fractured reservoirs. *Energies*. <https://doi.org/10.3390/en14175488>
- Baghbanan A, Jing L (2007) Hydraulic properties of fractured rock masses with correlated fracture length and aperture. *Int J Rock Mech Min Sci*. <https://doi.org/10.1016/j.ijrmms.2006.11.001>

- Barton N, Bandis S, Bakhtar K (1985) Strength, deformation and conductivity coupling of rock joints. *Int J Rock Mech Min Sci Geomech Abstr.* [https://doi.org/10.1016/0148-9062\(85\)93227-9](https://doi.org/10.1016/0148-9062(85)93227-9)
- Bear J, Tsang CF, de Marsily G (1993) Flow and contaminant transport in fractured rock. Academic Press, Boca Raton. <https://doi.org/10.1016/C2009-0-29127-6>
- Berkowitz B, Balberg I (1993) Percolation theory and its application to groundwater hydrology. *Water Resour Res.* <https://doi.org/10.1029/92WR02707>
- Berkowitz B (2002) Characterizing flow and transport in fractured geological media: a review. *Adv Water Resour.* [https://doi.org/10.1016/S0309-1708\(02\)00042-8](https://doi.org/10.1016/S0309-1708(02)00042-8)
- Beserra L, Guimarães L, Manzoli O (2016) Hydromechanical simulation of hydraulic fracturing in naturally fractured reservoir using strong discontinuity approach. In: 78th EAGE conference and exhibition. <https://doi.org/10.1190/sbgf2017-024>
- Beserra L, Guimarães L, Manzoli O, Alvarez L (2018) Finite element with embedded discontinuities analysis of well production decline due to fracture closure in naturally fractured reservoirs. In: ECMOR XVI - 16th European conference on the mathematics of oil recovery. <https://doi.org/10.3997/2214-4609.201802156>
- Bonnet E, Bour O, Odling N, Davy P, Main I, Cowie P, Berkowitz B (2001) Scaling of fracture systems in geological media. *Rev Geophys.* <https://doi.org/10.1029/1999RG000074>
- Cello A, Walker D, Valocchi A (2009) Flow dimension and anomalous diffusion of aquifer tests in fracture networks. *Vadose Zone J.* <https://doi.org/10.2136/vzj2008.0040>
- Charlaix E, Guyon E, Roux S (1987) Permeability of a random array of fractures of widely varying apertures. *Transp Porous Media.* <https://doi.org/10.1007/BF00208535>
- Couples G (2014) Geomechanical impacts on flow in fractured reservoirs. *Geol Soc London Spl Publ.* <https://doi.org/10.1144/sp374.17>
- Davy P, Bour O, Dreuzy J, Darcel C (2006) Flow in multiscale fractal fracture networks. *Geol Soc London Spl Publ.* <https://doi.org/10.1144/gsl.sp.2006.261.01.03>
- Davy P, Le Goc R, Darcel C, Bour O, Dreuzy J, Munier R (2010) A likely universal model of fracture scaling and its consequence for crustal hydromechanics. *J Geophys Res.* <https://doi.org/10.1029/2009JB007043>
- Decroux B, Gosselin O (2013) Computation of effective dynamic properties of naturally fractured reservoirs: comparison and validation of methods. EAGE Annu Conf Exhib Inc SPE Europec. <https://doi.org/10.3997/2214-4609.20130860>
- Dershowitz B, LaPointe P, Eiben T, Wei L (2000) Integration of discrete feature network methods with conventional simulator approaches. *SPE Reservoir Eval Eng.* <https://doi.org/10.2118/62498-PA>
- Dershowitz W, Fidelibus C (1999) Derivation of equivalent pipe network analogues for three-dimensional discrete fracture networks by the boundary element method. *Water Resour Res.* <https://doi.org/10.1029/1999WR900118>
- Dershowitz W, LaPointe P, Doe T (2004) Advances in discrete fracture network modeling.
- Dreuzy J, Davy P, Berkowitz B (2001) Advective transport in the percolation backbone in two dimensions. *Phys Rev E.* <https://doi.org/10.1103/PhysRevE.64.056305>
- Dreuzy J, Boiry P, Pichot G, Davy P (2010) Use of power averaging for quantifying the influence of structure organization on permeability upscaling in on-lattice networks under mean parallel flow. *Water Resour Res.* <https://doi.org/10.1029/2009WR008769>
- Dreuzy J, Méheust Y, Pichot G (2012) Influence of fracture scale heterogeneity on the flow properties of three-dimensional discrete fracture networks (DFN). *J Geophys Res Atmos.* <https://doi.org/10.1029/2012JB009461>
- Elfeel M (2014) Improved upscaling and reservoir simulation of enhanced oil recovery processes in naturally fractured reservoirs. Doctoral Dissertation, Heriot-Watt University.
- Erhel J, Dreuzy J, Bresciani E (2011) Multi-parametric intensive stochastic simulations for hydrogeology on a computational grid. *Parallel Comput Fluid Dyn.* [https://doi.org/10.1007/978-3-642-14438-7\\_41](https://doi.org/10.1007/978-3-642-14438-7_41)
- Evans D, Nicholson T, Rasmussen T (2001) Flow and transport through unsaturated fractured rock. *AGU Geophys Monogr Series.* <https://doi.org/10.1029/GM042p0001>
- Falcao F, Barroso J, Murad M et al (2018) Synthetic benchmark for the computation of equivalent properties in coupled flow-geomechanical Scenarios for a Fractured carbonate rock
- Fowler G, McClure M, Cipolla C (2019) a utica case study: the impact of permeability estimates on history matching, fracture length, and well spacing. *SPE Annu Tech Conf Exhib.* <https://doi.org/10.2118/195980-MS>
- Fraga C, Pinto A, Branco C, Pizarro J, Paulo C (2015) Brazilian pre-salt: an impressive journey from plans and challenges to concrete results. *Offshore Technol Conf.* <https://doi.org/10.4043/25710-MS>
- Frampton A, Cvetkovic V (2007) Upscaling particle transport in discrete fracture networks: 1. Nonreactive tracers. *Water Resour Res.* <https://doi.org/10.1029/2006WR005334>
- Frampton A, Cvetkovic V (2009) Significance of injection modes and heterogeneity on spatial and temporal dispersion of advecting particles in two-dimensional discrete fracture networks. *Adv Water Resour.* <https://doi.org/10.1016/j.advwatres.2008.07.010>
- Gao B, Flemings P (2017) Pore pressure within dipping reservoirs in overpressured basins. *Marine Petrol Geol.* <https://doi.org/10.1016/j.marpetgeo.2016.11.014>
- Kavousi Ghahfarokhi P, Wilson TH (2015) Fracture intensity attribute for the Tensleep reservoir at Teapot Dome, Wyoming, USA. *Interpretation* 3(3):41–48. <https://doi.org/10.1190/INT-2014-0258.1>
- Ghahfarokhi P (2017) The structured gridding implications for upscaling model discrete fracture networks (DFN) using corrected Oda's method. *J Petrol Sci Eng.* <https://doi.org/10.1016/j.petrol.2017.03.027>
- Golf-Racht TD (1982) Fundamentals of fractured reservoir engineering. Elsevier Science
- Guimarães L, Gens A, Olivella S (2007) Coupled thermo-hydro-mechanical and chemical analysis of expansive clay subjected to heating and hydration. *Transp Porous Media.* <https://doi.org/10.1007/s11242-006-0014-z>
- Gupta A, Penuela G, Avila R (2001) An integrated approach to the determination of permeability tensors for naturally fractured reservoirs. *J Can Pet Technol.* <https://doi.org/10.2118/01-12-02>
- Gutierrez M, Youn DJ (2015) Effects of fracture distribution and length scale on the equivalent continuum elastic compliance of fractured rock masses. *J Rock Mech Geotech Eng.* <https://doi.org/10.1016/j.jrmge.2015.07.006>
- Haridy M, Sedighi F, Ghahri P, Ussenova K, Zhiyenkulov M (2019) Comprehensive study of the Oda corrected permeability upscaling method. *SPE/IATMI Asia Pacific Oil and Gas Conference and Exhibition.* *SPE-196399-MS.* <https://doi.org/10.2118/196399-MS>
- Ji SH, Park YJ, Lee KK (2011) Influence of fracture connectivity and characterization level on the uncertainty of the equivalent permeability in statistically conceptualized fracture networks. *Transp Porous Media.* <https://doi.org/10.1007/s11242-010-9690-9>
- Jing L, Stephansson O (1997) Network topology and homogenization of fractured rocks. *Fluid Flow Transp Rocks.* [https://doi.org/10.1007/978-94-009-1533-6\\_11](https://doi.org/10.1007/978-94-009-1533-6_11)
- Latham J-P, Xiang J, Belayneh M, Nick MN, Tsang C-F, Blunt MJ (2013) Modelling stress-dependent permeability in fractured rock including effects of propagating and bending fractures. *Int J Rock Mech Min Sci* 57:100–112. <https://doi.org/10.1016/j.ijrmms.2012.08.002>

- Jourde H, Fenart P, Vinches M, Pistre S, Vayssade B (2007) Relationship between the geometrical and structural properties of layered fractured rocks and their effective permeability tensor. *J Hydrol*. <https://doi.org/10.1016/j.jhydrol.2007.01.027>
- Kalbacher T, Mettler R, McDermott C et al (2006) Geometric modelling and object-oriented software concepts applied to a heterogeneous fractured network from the Grimsel rock laboratory. *Comput Geosci*. <https://doi.org/10.1007/s10596-006-9032-8>
- Lang P, Paluszny A, Zimmerman R (2014) Permeability tensor of three-dimensional fractured porous rock and a comparison to trace map predictions. *J Geophys Res*. <https://doi.org/10.1002/2014JB011027>
- Le Goc R, Dreuzy J, Davy P (2010) Statistical characteristics of flow as indicators of channeling in heterogeneous porous and fractured media. *Adv Water Resour*. <https://doi.org/10.1016/j.advwatres.2009.12.002>
- Lei Q, Latham J, Tsang C (2017) The use of discrete fracture networks for modelling coupled geomechanical and hydrological behaviour of fractured rocks. *Comput Geotech*. <https://doi.org/10.1016/j.compgeo.2016.12.024>
- Leung C, Zimmerman R (2010) Estimating the hydraulic conductivity of two-dimensional fracture networks using effective medium theory and power-law averaging. *ISRM International Symposium*
- Li J, Lei Z, Qin G, Gong B (2015) Effective local-global upscaling of fractured reservoirs under discrete fractured discretization. *Energies*. <https://doi.org/10.3390/en80910178>
- Long J, Remer J, Wilson C, Witherspoon P (1982) Porous media equivalents for networks of discontinuous fractures. *Water Resour Res*. <https://doi.org/10.1029/WR018i003p00645>
- Long J, Gilmour P, Witherspoon P (1985) A model for steady fluid flow in random three-dimensional networks of disc-shaped fractures. *Water Resour Res*. <https://doi.org/10.1029/WR021i008p01105>
- Louguemare P, Mainguy M, Lemonnier P, Onaisi A, Gérard C, Koutsabeloulis N (2002) Geomechanics in reservoir simulation: overview of coupling methods and field case study. *Oil Gas Sci Technol*. <https://doi.org/10.1017/CBO9780511586477>
- Manzoli O, Shing P (2006) A general technique to embed non-uniform discontinuities into standard solid finite elements. *Comput Struct*. <https://doi.org/10.1016/j.compstruc.2005.10.009>
- Maryška J, Severýn O, Vohralík M (2004) Numerical simulation of fracture flow with a mixed-hybrid FEM stochastic discrete fracture network model. *Comput Geosci*. <https://doi.org/10.1007/s10596-005-0152-3>
- Mejia C, Roehl D, Rueda J, Fonseca F (2022) Geomechanical effects of natural fractures on fluid flow in a pre-salt field. *J Nat Gas Sci Eng*. <https://doi.org/10.1016/j.jngse.2022.104772>
- Narr W, Schechter D, Thompson L (2006) Naturally fractured reservoir characterization. Society of Petroleum Engineers. ISBN: 978-1-55563-112-3
- National Research Council (1996) Rock fractures and fluid flow: contemporary understanding and applications. The National Academies Press, Washington. <https://doi.org/10.17226/2309>
- National Research Council (2001) Conceptual models of flow and transport in the fractured vadose zone. The National Academies Press, Washington. <https://doi.org/10.17226/10102>
- Nelson RA (2001) Geologic analysis of naturally fractured reservoirs. Gulf Professional Publishing. ISBN 978-0-88415-317-7
- Niven E, Deutsch C (2009) A sensitivity analysis for equivalent permeability tensors calculated from 2D discrete fracture networks. CCG Annual Report.
- Nordqvist A, Tsang Y, Tsang C, Dverstorp B, Andersson J (1996) Effects of high variance of fracture transmissivity on transport and sorption at different scales in a discrete model for fractured rocks. *J Contam Hydrol*. [https://doi.org/10.1016/0169-7722\(95\)00064-X](https://doi.org/10.1016/0169-7722(95)00064-X)
- Oda M (1985) Permeability tensor for discontinuous rock masses. *Géotechnique*. <https://doi.org/10.1680/geot.1985.35.4.483>
- Oda M, Saitoo T, Kamemura K (1989) Permeability of rock masses at great depth. *ISRM International Symposium*. ISRM-IS-1989-057
- Olivella S, Carrera J, Gens A, Alonso E (1994) Nonisothermal multiphase flow of brine and gas through saline media. *Transp Porous Media*. <https://doi.org/10.1007/BF00613282>
- Olivella S, Gens A, Carrera J, Alonso E (1995) Numerical formulation for a simulator (CODE\_BRIGHT) for the coupled analysis of saline media. *Eng Comput*. <https://doi.org/10.1108/02644409610151575>
- Pan JB, Lee CC, Lee CH, Yeh HF, Lin H (2010) Application of fracture network model with crack permeability tensor on flow and transport in fractured rock. *Eng Geol*. <https://doi.org/10.1016/j.enggeo.2010.08.007>
- Pichot G, Erhel J, Dreuzy J (2010) A mixed hybrid Mortar method for solving flow in discrete fracture networks. *Appl Anal*. <https://doi.org/10.1080/00036811.2010.495333>
- Rubin Y, Hubbard S (2005) *Hydrogeophysics (Water science and Technology Library)*. Springer
- Rutqvist J, Stephansson O (2003) The role of hydromechanical coupling in fractured rock engineering. *Hydrogeol J*. <https://doi.org/10.1007/s10040-002-0241-5>
- Sahimi M (2011) Flow and transport in porous media and fractured rock: from classical methods to modern approaches. John Wiley & Sons, New York. <https://doi.org/10.1002/9783527636693>
- Sahimi M (1993) Flow phenomena in rocks: from continuum models to fractals, percolation, cellular automata, and simulated annealing. *Am Phys Soc*. <https://doi.org/10.1103/RevModPhys.65.1393>
- Sarma P, Aziz K (2006) New transfer functions for simulation of naturally fractured reservoirs with dual-porosity models. *SPE J*. <https://doi.org/10.2118/90231-PA>
- Sayers CM (1990) Stress-induced fluid flow anisotropy in fractured rock. *Transp Porous Media*. <https://doi.org/10.1007/BF00140017>
- Sævik P, Nixon C (2017) Inclusion of topological measurements into analytic estimates of effective permeability in fractured media. *Water Resour Res*. <https://doi.org/10.1002/2017WR020943>
- Shin H, Santamarina C (2019) An implicit joint-continuum model for the hydro-mechanical analysis of fractured rock masses. *Int J Rock Mech Min Sci*. <https://doi.org/10.1016/j.ijrmms.2019.04.006>
- Spence G, Couples G, Bevan T et al (2014) Advances in the study of naturally fractured hydrocarbon reservoirs: a broad integrated interdisciplinary applied topic. *Geol Soc London Spl Publ*. <https://doi.org/10.1144/sp374.19>
- Thibeau S, Mucha V (2011) Have we overestimated saline aquifer CO<sub>2</sub> storage capacities. *Oil Gas Sci Technol*. <https://doi.org/10.2516/ogst/2011004>
- Wellman T, Shapiro A, Hill M (2009) Effects of simplifying fracture network representation on inert chemical migration in fracture-controlled aquifers. *Water Resour Res*. <https://doi.org/10.1029/2008WR007025>
- Yan X, Huang Z, Yao J, Li Y, Fan D, Zhang K (2018) An efficient hydro-mechanical model for coupled multi-porosity and discrete fracture porous media. *Comput Mech*. <https://doi.org/10.1007/s00466-018-1541-5>
- Yeh T, Liu S (2000) Hydraulic tomography: development of a new aquifer test method. *Water Resour Res*. <https://doi.org/10.1029/2000WR900114>
- Zareidarmiyani A, Salarirad H, Vilarrasa V, Simone S, Olivella S (2018) Geomechanical response of fractured reservoirs. *Fluids*. <https://doi.org/10.3390/fluids3040070>
- Zimmerman R, Main I (2004) Hydromechanical behavior of fractured rocks. *Int Geophys*. [https://doi.org/10.1016/S0074-6142\(03\)80023-2](https://doi.org/10.1016/S0074-6142(03)80023-2)
- Zoback M (2007) Reservoir geomechanics. Cambridge University Press, Cambridge. <https://doi.org/10.1017/CBO9780511586477>